Tissue Antigens ISSN 0001-2815

Haplotyping of TNFα gene promoter using melting temperature analysis: detection of a novel –856(G/A) mutation

Y. Song[1], J. Araki[1], L. Zhang[1], T. Froehlich[2], M. Sawabe[3], T. Arai[3], T. Shirasawa[3] & M. Muramatsu[1]

1 Department of Molecular Epidemiology, Medical Research Institute, Tokyo Medical and Dental University, Chiyoda-ku, Tokyo, Japan
2 Roche Diagnostics GmbH, Roche Applied Science, Penzberg, Germany
3 Department of Pathology, Tokyo Metropolitan Institute of Gerontology

Key words
haplotyping; high throughput; melting temperature analysis; TNFα

Correspondence
Jungo Araki
Department of Molecular Epidemiology
Medical Research Institute
Tokyo Medical and Dental University
2-3-10 Kandasurugadai
Chiyoda-ku
Tokyo 101-0062
Japan
Tel: 81 3 5280 8060
Fax: 81 3 5280 8061
e-mail: araju.epi@mri.tmd.ac.jp

Received 27 March 2005; revised 31 May 2005; accepted 20 June 2005

doi: 10.1111/j.1399-0039.2005.00464.x

Abstract

Tumor necrosis factor alpha (TNFα) is a potent cytokine with a wide range of pro-inflammatory activities and plays a critical role in the pathogenesis of a number of infectious, inflammatory, autoimmune, and metabolic diseases. We determined four single-nucleotide polymorphisms (SNPs), –1031(C/T), –863(C/A), –857(C/T), and –308(G/A) in the TNFα promoter region using melting temperature analysis, among 1451 geriatric autopsy samples. Two adjacent SNPs, –863(C/A) and –857(C/T), were directly assayed by a single probe reaction, which correctly determined three of four expected haplotypes. Sequence confirmation related that the most rare haplotype (8/2902 chromosomes, frequency: 0.26%) contains a novel mutation of –856(G/A), instead of the predicted haplotype. These results indicate that melting temperature analysis provides a robust method to determine the polymorphisms in the TNFα promoter.

Introduction

Tumor necrosis factor alpha (TNFα) is a potent cytokine with a wide range of pro-inflammatory activities and plays a critical role in protection from microbial infection and in the pathogenesis of a number of inflammatory or autoimmune diseases. Polymorphisms of the *TNFα* gene have been repeatedly employed in association studies of various diseases (1–3), such as systemic lupus erythematosus (4, 5), viral infection (6), shizophrenia (7), endometriosis (8), inflammatory polyarthritis (9), bone mineral density (10), asthma (11), and rheumatoid arthritis (12, 13). Especially, single-nucleotide polymorphisms (SNPs) in the promoter region that may account for transcriptional regulation and production of TNFα have attracted attention. Not only individual SNPs but also haplotypes, defined by these SNPs, have been subjected to analysis (8, 14–20). Indeed, there are previous attempts to directly haplotype the TNFα promoter region such as using polymerase chain reaction (PCR)-preferential homoduplex formation assay (PCR-PHFA) (21).

In this study, we employed melting temperature analysis, which has been proved to be useful for genotyping SNPs (22, 23), for detecting polymorphisms in the TNFα promoter region. We applied this method to analyze the polymorphisms –1031(C/T) (rs1799964), –863(C/A) (rs1800630), –857(C/T) (rs1799724), and –308(G/A) (rs1800629) in the TNFα promoter and showed that it is a robust method. Of note is that this method allowed direct haplotyping of –863(C/A) and –857(C/T) in a single tube reaction. In the course of sequence confirmation, we unexpectedly found that the most rare haplotype, which occurred at the frequency of 8/2902 (0.26%), contained a novel mutation of G to A at the position –856 in the TNFα promoter.

Materials and methods

Samples

DNA samples were obtained from patients in Tokyo Metropolitan Institute of Gerontology with appropriate informed consent and partially published in the article (24). This study was approved by the ethical committee of Tokyo Metropolitan Geriatric Medical Center and Tokyo Medical and Dental University. A total of 1451 genomic DNA samples were used for the analysis. Genomic DNA was extracted from the renal cortex by the phenol-chloroform method and kept at –20°C until usage. For the genotyping reaction, 10 ng of DNA aliquots were placed in 384-well PCR plates using automated fluid dispenser (BioMek2000, Beckman Coulter Inc, Fullerton, CA) and was dried down in a dry chamber.

Melting temperature analysis protocol

PCR for –863 and –857 haplotype region, –1031 and –308 SNP regions

To assay the haplotype for TNFα [–863(C/A) and –857(C/T)], we synthesized PCR primers and FRET-probes (Table 1). The PCR amplification reaction was done in 5 μl volume using LightTyper 384 PCR kit (Roche Diagnostics, Penzberg, Germany). Each well contained 1 × PCR buffer, 3 mM $MgCl_2$, 1 mM dNTP, 0.05 μM upstream primer, 1 μM downstream primer, 0.2 μM anchor probe, 0.2 μM detection probe, 0.5 U Faststart Taq polymerase, and dried-down 10 ng of DNA. To assay –1031(C/T) and –308(G/A), we synthesized other sets of PCR primers and probes (Table 1). The PCR amplification reaction was essentially the same, except that the primer concentration was 0.025 and 0.5 μM, respectively. PCR is performed in a GeneAmp PCR system 9700 (Applied Biosystems Inc, Foster City, CA) with a cycling protocol of initial denaturation at 94°C for 10 min, followed by 40 cycles of 94°C for 15 s, 55°C for 15 s, and 72°C for 15 s and final extension step at 72°C for 10 min.

Melting temperature analysis

Melting temperature analysis was done on the LightTyper Instrument (Roche Diagnostics). After completion of PCR, denaturation and annealing as preamble to melting were done by heating the mixture at 94°C for 60 s and then kept at 40°C for 60 s. Then the plates were heated from 40 to 90°C by the gradient of 0.1°C/s. Melting temperature data were collected and classified using the LIGHTTYPER GENOTYPING software, and call for genotypes and haplotypes was made. The melting temperature results were further checked by eye inspection when necessary.

TA cloning

Genomic DNA of selected samples was amplified using the same primer (Table 1), and PCR products of interest were separated by agarose gel electrophoresis. PCR products were extracted and purified by gel filtration (Wizard SV Gel and PCR Clean-Up System, Promega Corporation, Madison, WI) and were subcloned into a TA cloning vector (pGEM-T and pGEM-T Easy Vector Systems, Promega Corporation). Several individual clones for each sample were isolated and sequence was determined.

Sequencing

Sequencing of the DNA fragments was performed using a standard procedure for ABI 3100 capillary sequencer (Applied Biosystems Inc). In brief, PCR was performed

Table 1

Target polymorphisms		Sequence
–1031(C/T) SNP	Forward primer	5′-GGTCCTACACACAAATCAGTC
	Reverse primer	5′-CTTCTGTCTCGGTTTCTTCTC
	Anchor probe	5′-AGGATACCCCTCACACTCCCCATC-fluorescein
	Detection probe	5′ LC Red 640-CCCTGCTCCGATTCCGAG-phosphate
–863(C/A) and –857(C/T) haplotype	Forward primer	5′-GGCTCTGAGGAATGGGTTAC
	Reverse primer	5′-AGTGTGTGGCCATATCTTCTTAAA
	Anchor probe	5′ LC Red 640-GGGCCATGTAGAGGGCCC-phosphate
	Detection probe	5′-GGGACCCCCCCTTAATGAAGA-fluorescein
–308(G/A) SNP	Forward primer	5′-GAGATGTGACCACAGCAA
	Reverse primer	5′-TATCTTCTTAAACGTCCCCTGTATT
	Anchor probe	5′ LC Red 640-TGTAGAGGGCCCCAGGGAGT-phosphate
	Detection probe	5′-CCCCCTTAACGAAGACAGGGC-fluorescein

SNP, single-nucleotide polymorphism.
The base with underbars corresponds to the SNP site.

in 10 μl of reaction mixture containing 20 ng of genomic DNA, 0.2 μl of Faststart Taq DNA polymerase, and the same concentrations of the other reagents as described above. For direct sequencing from genome, DNA was PCR amplified and purified by gel extraction, and dye terminator reaction was performed.

Melting temperature estimation

The melting temperature was estimated by the nearest-neighbor method (25). In principle, the whole enthalpy and entropy of DNA double strand constructed between probe and amplicon, or primer and genome template, are approximated to the sum of two base units. The enthalpy and entropy for the matches and mismatches of the two base units are derived from experimental data (26). The calculation for the melting temperature was done by a software, MELTING (27).

Haplotype estimation

To infer haplotype consisting of three SNPs [–1031(C/T), –863(C/A) and –857(C/T)], we used haplo.stat package (Jason P. Sinnwell and Daniel J. Schaid in Mayo Foundation for Medical Education and Research) that is written in the R language. The data for the haplotype directly determined for –863(C/A) and –857(C/T) and genotype data for 1031(C/T) were used.

Results

Molecular haplotyping of –863(C/A) and –857(C/T)

The accuracy of melting temperature analysis using probes with combination of base mismatch is the key to this haplotyping. The probe used for the analysis contained G and A at the bases corresponding to –863 and –857, respectively (Table 1). Accordingly, the melting temperatures for the haplotypes, -C-T-, -C-C-, -A-T- and -A-C-, were calculated to be 65.8, 62.9, 56.4, and 52.6°C, respectively, by MELTING (Table 2).

Typical curve patterns for allelic discrimination are shown in Figure 2. Overall, there were four melting temperature peaks detected in the melting temperature curves, which were 63.7 ± 0.5 (mean ± SD), 60.2 ± 0.5, 53.7 ± 0.4, and 51.1 ± 0.4° C, that correspond to the estimated Tm of 65.8, 62.9, 57.9 and 52.6° C (Figure 2). One DNA sample gave rise to one melting temperature curve, which shows either one or two peaks which were meant to be homozygous or heterozygous for a combination of haplotypes (diplotype) (Figure 3). By the combination of appearing peaks, nine typical melting temperature curve patterns were detected from the analysis of 1451 DNA samples, which correspond to nine of 10 possible diplotypes, that is 1/1, 1/2, 1/3, 1/4, 2/2, 2/3, 2/4, 3/4, and 4/4. The frequencies of haplotypes 1, 2, 3, and 4 were 15.9, 67.1, 0.3, and 16.8%, respectively.

Sequence confirmation reveals a novel mutation –856(G/A)

To confirm the haplotyping results, we determined the sequence of the corresponding region. We randomly selected samples from each haplotype combination and direct genomic sequencing, or sequencing DNA fragments after cloning into a TA vector, were performed. The 5 sequences for samples from 1/1, 1/2, 1/4, 2/2, 2/4, and 4/4 were totally consistent with the SNP calls obtained by melting temperature analysis (data not shown). This indicated that determination of haplotypes 1, 2 and 4 by this method is accurate.

We then sequenced all of the eight samples of 1/3, 2/3, and 3/4 that were predicted to have haplotype 3. By sequencing the DNA fragment obtained by TA cloning, we confirmed the existence of haplotype 1, 2 and 4, respectively. However, the sequence of haplotype 3 was not as predicted but included a novel mutation of G to A at the position –856 (Figure S1, *Supplementary Material*). All of the eight samples that carried haplotype 3 contain a sequence with the same mutation. Thus, we concluded that haplotype 3 is correctly (–863C)–(–857C)–(–856A), which is equivalent to having –856G to A mutation on haplotype 2. Because the frequency of –856(G/A) is less than 1%, by definition, it is a new mutation rather than a polymorphism. This new mutation is registered in GenBank with the accession number of AB196340.

19 **Table 2**

	TNFα			
	–863	–857	Expected Tm	Observed Tm (mean SD)
Haplotype 1	C	T	65.8	63.7 ± 0.5
Haplotype 2	C	C	62.9	60.2 ± 0.5
Haplotype 3	A	T	56.4	53.7 ± 0.4
Haplotype 4	A	C	52.6	51.1 ± 0.4

20 Haplotype 3 was shown to contain a cryptic mutation by sequence analysis (see text).

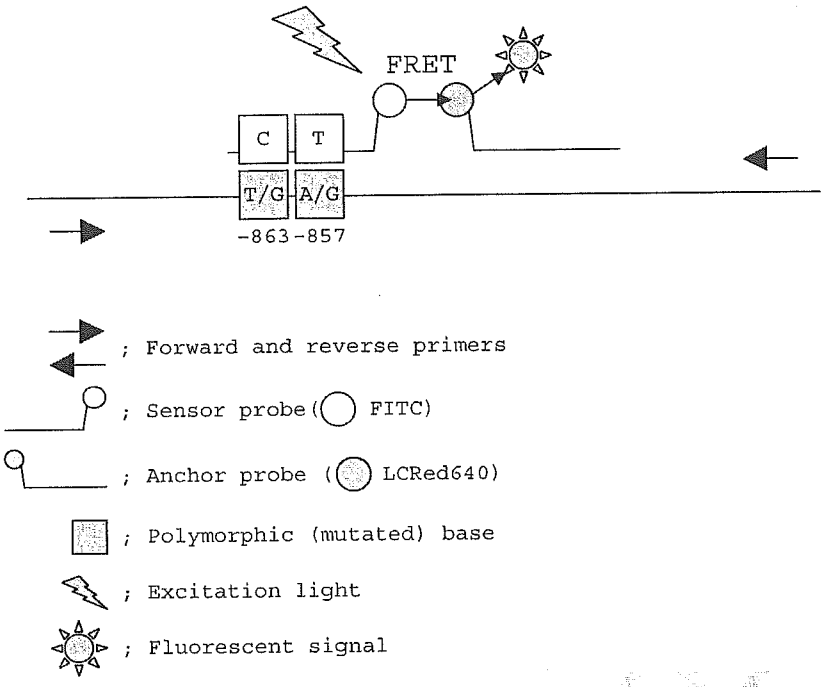

Figure 1 A schema of probe and primer sets to detect –863(A/C)/857(C/T) haplotype by melting temperature analysis. Combination of two single-nucleotide polymorphisms would generate different Tm between sensor probe and the amplicon.

16

SNP typing of –1031(C/A) and –308(G/A)

We further determined two other SNPs, –1031(C/A) and –308(G/A), in the TNFα promoter using the probes and primers summarized in Table 1. The genotype frequency of –1031(C/T) was TT: 3.03%, TC: 30.19%, and CC: 66.78%, and the allele frequency of T : C was 18.13: 81.87% (Table 4). The –1031(C/T) SNP conveyed the Hardy–Weinberg equilibrium (P = 0.596). The genotype frequency of –308(G/A) was GG: 98.19%, GA: 0.98%, and AA: 0.14%, and the allele frequency was G : A = 99.02: 0.98% (Table 3). The –308 (G/A) SNP did not convey the Hardy–Weinberg equilibrium (P = 0.0004).

We then combined the typing data of –863(C/A)-–857(C/T), and –1031 (C/T) to construct haplotype of these three SNPs by using haplo.stat. The typing data for –308(G/A) were not used, as the minor allele frequency was low and it did not convey the Hardy–Weinberg equilibrium. In this analysis, haplotypes 2 and 3 were

6

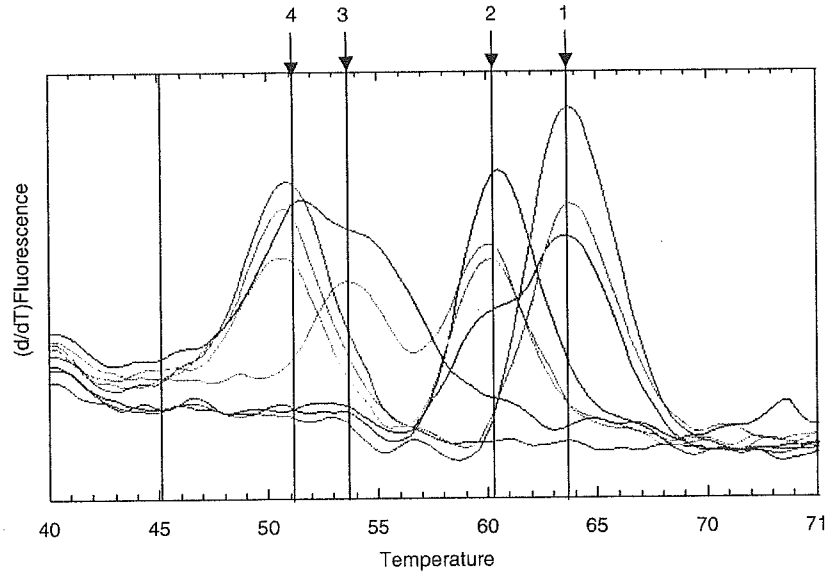

25

Figure 2 Representative melting temperature curves from the analysis of 1451 samples. Collectively, four melting temperature peaks were observed, which correspond to the predicted four melting temperatures. Melting temperature curves and corresponding haplotype numbers are shown.

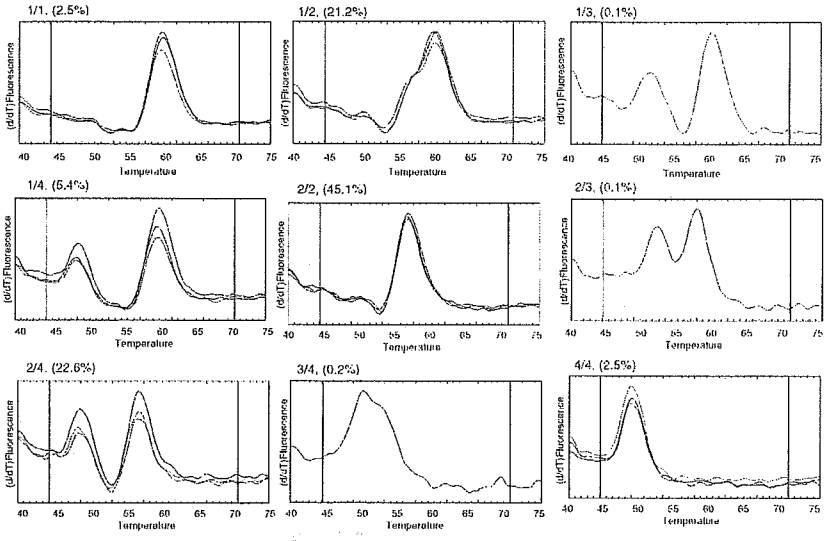

Figure 3 Individual melting temperature curve profiles for nine diplotypes. 1/1, 1/2, 1/3 (top, left to right), 1/4, 2/2, 2/3 (middle, left to right), 2/4, 3/4 and 4/4 (bottom, left to right) are shown. Three sample traces are shown for each diplotype except for 1/3, 2/3 and 3/4. The frequency of each diplotype among 1451 samples is shown in the parentheses.

7 combined and treated as –863(C)- –857(C) haplotype. The frequency of haplotypes consisted with –1031(C/T), 8 –863(C/A), 857(C/T) in our 1451 samples is summarized in Table 4. The frequencies of haplotypes and combination of haplotypes were compatible with Hardy–Weinberg equilibrium (data not shown). The frequency of haplotype in our sample was compatible with that previously reported for a Japanese population by Matsushita et al. (Table 4).

Discussion

Using melting temperature analysis, we have analyzed the polymorphisms in the TNFα promoter. We have shown that this method is robust and suitable for high-throughput SNP typing. Also, targeting two SNPs on a single probe, we could determine three of four haplotypes by this method.

SNP genotyping is now a key technology for genetic studies in public research with major impact on epidemiology, pharmacogenomics, drug discovery, and forensic sciences. A large number of SNPs in the human genome have been identified (28), and this information is integrated into linkage disequilibrium and haplotype patterns (29). Haplotype phase is expected to provide more valuable information than individual SNPs, with regard to genetic history and correlating genetic variants involved in susceptibility to human diseases (30). It has been suggested that haplotypes might be more appropriate for pharmacogenetic assessment (30–32), when SNPs contributing to distinct trait are not directly observed, the effects of observed SNPs are non-additive, and when haplotype is 9 directly contributing to disease phenotype (33). Although haplotype is usually inferred from non-familial population using computer-based methods, such as parsimony (34), expectation-maximization algorithm (35), and Bayesian methods (36), molecular methods to directly determine haplotypes, molecular haplotyping, are required. Most straightforward procedure is to clone and sequence the two homologous chromosome regions (37), but this is usually too labor intensive and high cost. Allele-specific PCR in combination with hybridization to sequence-specific oligonucleotides (38), or with restriction fragment length polymorphism analysis (39,40), were also applied for haplotyping up to several SNPs (41–48). However, these methods are also not sufficiently robust for high-throughput typing.

The procedure for molecular haplotyping by melting temperature analysis is essentially the same as genotyping a single SNP. It requires only two steps, PCR followed by fluorescent detection. After PCR set-up, the homogenous assay is carried out in a closed microtiter plate. No post-

21 **Table 3**

22

TNFα locus	n = 1451	Genotype frequency (%)
–1031		
TT	969	3.03
TC	438	30.19
CC	44	66.78
–863		
CC	1005	69.26
AC	410	28.26
AA	36	2.48
–857		
CC	1025	70.64
CT	390	26.88
TT	36	2.48
–308		
GG	1407	98.19
GA	24	1.67
AA	2	0.14

[24] [23] **Table 4**

−1031(C/T)- −863(C/A)- −857(C/T)- −856(G/A)	Haplotype frequency from this study (n = 1451) (%)	Haplotype frequency cited from Matsushita et al. 1999 (21), (n = 271) (%)
-T-C-C-G- (haplotype 2)	65.7	66.1
-C-A-C-G- (haplotype 4)	16.6	13.8
-T-C-T-G- (haplotype 1)	15.9	17.5
-C-C-C-G- (haplotype 2)	1.5	2.6
-T-C-C-A- (haplotype 3)	1.4	–
-C-C-T-G- (haplotype 1)	0.0	–

PCR manipulation of amplified samples is required, and therefore, this method can easily be implemented in a high-throughput platform. After placing all samples and reagents in a 384-well plate, it took only 3 h to obtain the melting temperature curve and SNP call.

Although our results demonstrated the feasibility of this method for high-throughput molecular haplotyping, a drawback was apparent as well. In this study, one rare haplotype (haplotype 3) was not as predicted but contained a previously unknown mutation. This happened because the Tm for the predicted haplotype 3 allele (56.4° C) and that for the actual mutation containing allele(57.9° C) are close. Therefore, it should be pointed out that when setting up an assay, confirmatory test by sequencing is necessary. Once the condition is set, this method can robustly be applied for high-throughput detection of haplotypes and mutation.

[10] Supplementary Material

Figure S1. Sequence analysis of haplotype 3. DNA samples which posses haplotype 3 were sequenced by TA cloning or direct sequencing. (A) Sequencing result of 1/3 sample after TA cloning. (B) Sequencing result of 3/4 sample after TA cloning. (C) Direct sequencing of 2/3 sample. –863 and –857 SNPs are shown by black arrows, and –856 G/A mutation is shown by an open arrow.

This material is available as part of the online article from http://www.blackwell-synergy.com

References

1. Bidwell J, Keen L, Gallagher G et al. Cytokine gene polymorphism in human disease: on-line databases. *Genes Immun* 1999: **1**: 3–19.
2. Bidwell J, Keen L, Gallagher G et al. Cytokine gene polymorphism in human disease: on-line databases, supplement 1. *Genes Immun* 2001: **2**: 61–70.
3. Haukim N, Bidwell JL, Smith AJ et al. Cytokine gene polymorphism in human disease: on-line databases, supplement 2. *Genes Immun* 2002: **3**: 313–30.
4. Tsuchiya N, Kawasaki A, Tsao BP, Komata T, Grossman JM, Tokunaga K. Analysis of the association of HLA-DRB1, TNFalpha promoter and TNFR2 (TNFRSF1B) polymorphisms with SLE using transmission disequilibrium test. *Genes Immun* 2001: **2**: 317–22.
5. Zuniga J, Vargas-Alarcon G, Hernandez-Pacheco G, Portal-Celhay C, Yamamoto-Furusho JK, Granados J. Tumor necrosis factor-alpha promoter polymorphisms in Mexican patients with systemic lupus erythematosus (SLE). *Genes Immun* 2001: **2**: 363–6.
6. Kim YJ, Lee HS, Yoon JH et al. Association of TNF-alpha promoter polymorphisms with the clearance of hepatitis B virus infection. *Hum Mol Genet* 2003: **12**: 2541–6.
7. Duan S, Xu Y, Chen W et al. No association between the promoter variants of tumor necrosis factor alpha (TNF-alpha) and schizophrenia in Chinese Han population. *Neurosci Lett* 2004: **366**: 139–43.
8. Teramoto M, Kitawaki J, Koshiba H et al. Genetic contribution of tumor necrosis factor (TNF) -alpha gene promoter (-1031-863 and -857) and TNF receptor 2 gene polymorphisms in endometriosis susceptibility. *Am J Reprod Immunol* 2004: **51**: 352–7.
9. Barton A, Platt H, Salway F et al. Polymorphisms in the tumour necrosis factor gene are not associated with severity of inflammatory polyarthritis. *Ann Rheum Dis* 2004: **63**: 280–4.
10. Furuta I, Kobayashi N, Fujino T et al. Bone mineral density of the lumbar spine is associated with TNF gene polymorphisms in early postmenopausal Japanese women. *Calcif Tissue Int* 2004: **74**: 509–15.
11. Noguchi E, Yokouchi Y, Shibasaki M et al. Association between TNFA polymorphism and the development of asthma in the Japanese population. *Am J Respir Crit Care Med* 2002: **166**: 43–6.
12. Mulcahy B, Waldron-Lynch F, McDermott MF et al. Genetic variability in the tumor necrosis factor-lymphotoxin region influences susceptibility to rheumatoid arthritis. *Am J Hum Genet* 1996: **59**: 676–83.
13. Waldron-Lynch F, Adams C, Amos C et al. Tumour necrosis factor 5′ promoter single nucleotide polymorphisms influence susceptibility to rheumatoid arthritis (RA) in immunogenetically defined multiplex RA families. *Genes Immun* 2001: **2**: 82–7.
14. Date Y, Seki N, Kamizono S et al. Identification of a genetic risk factor for systemic juvenile rheumatoid arthritis in the 5′-flanking region of the TNFalpha gene and HLA genes. *Arthritis Rheum* 1999: **42**: 2577–82.
15. Endo M, Tai H, Tabeta K, Kobayashi T, Yamazaki K, Yoshie H. Analysis of single nucleotide polymorphisms in the 5′-flanking region of tumor necrosis factor-alpha gene in Japanese patients with early-onset periodontitis. *J Periodontol* 2001: **72**: 1554–9.
16. Grutters JC, Sato H, Pantelidis P et al. Increased frequency of the uncommon tumor necrosis factor -857T allele in British and Dutch patients with sarcoidosis. *Am J Respir Crit Care Med* 2002: **165**: 1119–24.
17. Higuchi T, Seki N, Kamizono S et al. Polymorphism of the 5′-flanking region of the human tumor necrosis factor (TNF)-alpha gene in Japanese. *Tissue Antigens* 1998: **51**: 605–12.

18. Lee S-G, Kim B, Yook J-H, Oh S-T, Lee I, Song K. TNF/LTA polymorphisms and risk for gastric cancer/duodenal ulcer in the Korean population. *Cytokine* 2004: **28**: 75–82.
19. Park YJ, Park H, Park MH. TNF-alpha promoter polymorphisms and extended HLA and TNF-alpha haplotypes in Koreans based on 100 families. *Tissue Antigens* 2004: **63**: 75–9.
20. Negoro K, McGovern DPB, Kinouchi Y et al. Analysis of the IBD5 locus and potential gene-gene interactions in Crohn's disease. *Gut* 2003: **52**: 541–6.
21. Matsushita M, Tsuchiya N, Nakayama T et al. Allele typing of human TNFA 5′-flanking region using polymerase chain reaction-preferential homoduplex formation assay (PCR-PHFA): linkage disequilibrium with HLA class I and class II genes in Japanese. *Tissue Antigens* 1999: **54**: 478–84.
22. Bennett CD, Campbell MN, Cook CJ et al. The lighttyper: high-throughput genotyping using fluorescent melting curve
11 analysis. *Biotechniques* 2003: **34**: 1288–92, 1294–85.
23. Didenko VV. DNA probes using fluorescence resonance energy transfer (FRET): designs and applications.
12 *Biotechniques* 2001: **31**: 1106–16, 1118, 1120–1101.
24. Sawabe M, Arai T, Kasahara I et al. Developments of geriatric autopsy database and internet-based database of Japanese single nucleotide polymorphisms for geriatric research (JG-SNP). *Mech Ageing Dev* 2004: **125**: 547–52.
25. Panjkovich A, Melo F. Comparison of different melting temperature calculation methods for short DNA sequences.
13 Bioinformatics 2004.
26. SantaLucia J Jr. A unified view of polymer, dumbbell, and oligonucleotide DNA nearest-neighbor thermodynamics. *Proc Natl Acad Sci USA* 1998: **95**: 1460–5.
27. Le Novere N. MELTING, computing the melting temperature of nucleic acid duplex. *Bioinformatics* 2001: **17**: 1226–7.
28. Sachidanandam R, Weissman D, Schmidt SC et al. A map of human genome sequence variation containing 1.42 million single nucleotide polymorphisms. *Nature* 2001: **409**: 928–33.
29. Gabriel SB, Schaffner SF, Nguyen H et al. The structure of haplotype blocks in the human genome. *Science* 2002: **296**: 2225–9.
30. McCarthy JJ, Hilfiker R. The use of single-nucleotide polymorphism maps in pharmacogenomics. *Nat Biotechnol* 2000: **18**: 505–8.
31. Davidson S. Research suggests importance of haplotypes over SNPs. *Nat Biotechnol* 2000: **18**: 1134–5.
32. Drysdale CM, McGraw DW, Stack CB et al. Complex promoter and coding region beta(2) -adrenergic receptor haplotypes alter receptor expression and predict in vivo responsiveness. *Proc Natl Acad Sci USA* 2000: **97**: 10483–8.
33. Judson R, Stephens JC. Notes from the SNP vs. haplotype front. *Pharmacogenomics* 2001: **2**: 7–10.
34. Clark AG. Inference of haplotypes from PCR-amplified samples of diploid populations. *Mol Biol Evol* 1990: **7**: 111–22.
35. Excoffier L, Slatkin M. Maximum-likelihood estimation of molecular haplotype frequencies in a diploid population. *Mol Biol Evol* 1995: **12**: 921–7.
36. Stephens M, Smith NJ, Donnelly P. A new statistical method for haplotype reconstruction from population data. *Am J Hum Genet* 2001: **68**: 978–89.
37. Martinez-Arias R, Bertranpetit J, Comas D. Determination of haploid DNA sequences in humans: application to the glucocerebrosidase pseudogene. *DNA Seq* 2002: **13**: 9–13.
38. Boldt ABW, Petzl-Erler ML. A new strategy for mannose-binding lectin gene haplotyping. *Hum Mutat* 2002: **19**: 296–306.
39. McDonald OG, Krynetski EY, Evans WE. Molecular haplotyping of genomic DNA for multiple single-nucleotide polymorphisms located kilobases apart using long-range polymerase chain reaction and intramolecular ligation. *Pharmacogenetics* 2002: **12**: 93–9.
40. Woolley AT, Guillemette C, Cheung CL, Housman DE, Lieber CM. Direct haplotyping of kilobase-size DNA using carbon nanotube probes. *Nat Biotechnol* 2000: **18**: 760–3.
41. Chang SYA, Yang PC. On uniqueness of solutions of n-TH order differential equations in conformal geometry. *Math Res Lett* 1997: **4**: 91–102.
42. Eitan Y, Kashi Y. Direct micro-haplotyping by multiple double PCR amplifications of specific alleles (MD-PASA). *Nucleic Acids Res* 2002: **30**. 14
43. Koss K, Fanning GC, Welsh KI, Jewell DP. Interleukin-10 gene promoter polymorphism in English and Polish healthy controls. Polymerase chain reaction haplotyping using 3′ mismatches in forward and reverse primers. *Genes Immun* 2000: **1**: 321–4.
44. Lo YM, Patel P, Newton CR, Markham AF, Fleming KA, Wainscoat JS. Direct haplotype determination by double ARMS: specificity, sensitivity and genetic applications. *Nucleic Acids Res* 1991: **19**: 3561–7.
45. Newton CR, Graham A, Heptinstall LE et al. Analysis of any point mutation in DNA. The amplification refractory mutation system (ARMS). *Nucleic Acids Res* 1989: **17**: 2503–16.
46. Okimoto R, Dodgson JB. Improved PCR amplification of multiple specific alleles (PAMSA) using internally mismatched primers. *Biotechniques* 1996: **21**: 20–&. 15
47. Ruano G, Kidd KK. Direct haplotyping of chromosomal segments from multiple heterozygotes via allele-specific PCR amplification. *Nucleic Acids Res* 1989: **17**: 8392.
48. Sarkar G, Sommer SS. Haplotyping by double PCR amplification of specific alleles. *Biotechniques* 1991: **10**: 436, 438, 440.

THE JOURNAL OF BIOLOGICAL CHEMISTRY
Vol. 280, No. 16, Issue of April 22, pp. 16417–16426, 2005
Printed in U.S.A.
© 2005 by The American Society for Biochemistry and Molecular Biology, Inc.

Estrogen, Insulin, and Dietary Signals Cooperatively Regulate Longevity Signals to Enhance Resistance to Oxidative Stress in Mice*

Received for publication, January 25, 2005, and in revised form, February 15, 2005
Published, JBC Papers in Press, February 15, 2005, DOI 10.1074/jbc.M500924200

Tomonori Baba‡§, Takahiko Shimizu‡, Yo-ichi Suzuki‡, Midori Ogawara‡, Kyo-ichi Isono¶‖, Haruhiko Koseki¶‖, Hisashi Kurosawa§, and Takuji Shirasawa‡**

From the ‡Department of Molecular Gerontology, Tokyo Metropolitan Institute of Gerontology, Itabashi-ku, Tokyo, 173-0015, Japan, ¶Molecular Embryology, Graduate School of Medicine, Chiba University, Chiba, 260-8670, Japan, and §Department of Orthopedics, Juntendo University, Bunkyo-ku, Tokyo, 113-8421, Japan

To investigate the biological significance of a longevity mutation found in *daf-2* of *Caenorhabditis elegans*, we generated a homologous murine model by replacing Pro-1195 of insulin receptors with Leu using a targeted knock-in strategy. Homozygous mice died in the neonatal stage from diabetic ketoacidosis, whereas heterozygous mice showed the suppressed kinase activity of the insulin receptor but grew normally without spontaneously developing diabetes during adulthood. We examined heterozygous insulin receptor mutant mice for longevity phenotypes. Under 80% oxygen, mutant female mice survived 33.3% longer than wild-type female mice, whereas mutant male mice survived 18.2% longer than wild-type male mice. These results suggested that mutant mice acquired more resistance to oxidative stress, but the benefit of the longevity mutation was more pronounced in females than males. Manganese superoxide dismutase activity in mutant mice was significantly up-regulated, suggesting that the suppressed insulin signaling leads to an enhanced antioxidant defense. To analyze the molecular basis of the gender difference, we administered estrogen to mutant mice. It was found that the survival of mice under 80% oxygen was extended when they were administered estradiol. In contrast, mutant and wild-type female mice showed shortened survivals when their ovaries were removed. The influence of estrogen is remarkable in mutant mice compared with wild-type mice, suggesting that estrogen modulates insulin signaling in mutant mice. Furthermore, we showed additional extension of survival under oxidative conditions when their diet was restricted. Collectively, we show that three distinct signals; insulin, estrogen, and dietary signals work in independent and cooperative ways to enhance the resistance to oxidative stress in mice.

Recent experimental evidence suggests that oxidative stress is a principle cause of aging (1). Biochemical data further support the hypothesis that the oxidative damage accumulated in macromolecules such as DNAs, lipids, and proteins leads to the physiological decline in aging tissues. In a genetic analysis of invertebrate models, longevity mutants have been identified that show extension of lifespan associated with an enhanced resistance to oxidative stress (2). In *Caenorhabditis elegans*, a mutation of the *daf-2* gene that encodes an insulin/insulin-like growth factor type 1 (IGF-1)[1] receptor significantly enhanced resistance to oxidative stress and extended lifespan (3). These phenotypes are regulated by the insulin/IGF-1 signaling pathway from DAF-2 to DAF-16, a homologue of the hepatocyte nuclear factor-3/forkhead transcription factor (4, 5). Furthermore, expression of *sod3* encoding manganese superoxide dismutase (MnSOD) is up-regulated in *daf-2* mutants (5). In insulin-like signaling mutants of flies, it is suggested that the increased expression of SOD genes confers resistance to oxidative stress and the extension of lifespan (6). Thus, the regulation of SOD levels is critical for the determination of lifespan, which is modified by the insulin/IGF-1 signaling pathway. This signaling pathway has evidently been conserved from *C. elegans* to *Drosophila* (5, 6).

Holzenberger *et al.* (7) reported that a heterozygous deficiency for the IGF-1 receptor in mice enhances resistance to oxidative stress and extends lifespan. Because in IGF-1 receptor deficient mice heterozygous females exhibited a greater increase in lifespan than males, the beneficial effect of reduced IGF-1 signaling is also modulated by gender difference. However, it is unclear whether insulin signaling controls tolerance to oxidative stress and the extension of lifespan in mammals or is modulated by gender difference. In humans, the life expectancy of women is generally longer than that of men. For example, in Japan, with the highest life expectancy in the world, life expectancy was 78.36 years for men and 85.33 years for women in 2003. However, in laboratory animal models, the relationship of gender to longevity is variable, with lifespan being dependent on other factors like breeding and diet (8). Borras *et al.* (9) paid attention to the gender difference in rats, reporting that the expression and enzyme activity levels of MnSOD as well as glutathione peroxidase are higher in females than males. Ho *et al.* (10) reported that human MnSOD transgenic mice showed a significant increase in survival when exposed to 90% oxygen. Furthermore, in pulmonary epithelial cells of mice the overexpression of human MnSOD confers protection

* This work was supported by grants for Comprehensive Research on Aging and Health from the Ministry of Health, Labor, and Welfare. The costs of publication of this article were defrayed in part by the payment of page charges. This article must therefore be hereby marked "*advertisement*" in accordance with 18 U.S.C. Section 1734 solely to indicate this fact.

‖ Present address: Dept. of Developmental Genetics, Riken Research Center for Allergy and Immunology, Kanagawa, 230–0045, Japan.

** To whom correspondence should be addressed: Dept. of Molecular Gerontology, Tokyo Metropolitan Institute of Gerontology, 35-2 Sakaecho, Itabashi-ku, Tokyo 173-0015, Japan. Tel.: 81-3-3964-3241; Fax: 81-3-3579-4776; E-mail: sirasawa@tmig.or.jp.

[1] The abbreviations used are: IGF-1, insulin-like growth factor type 1; AL, *ad libitum*; Cu/ZnSOD, copper/zinc superoxide dismutase; MnSOD, manganese superoxide dismutase; DR, dietary restriction; E2, 17β-estradiol; IR, insulin receptor; OVX, ovariectomy; ROS, reactive oxygen species; wt, wild type; kb, kilobase; RT, reverse transcription.

against exposure to hyperoxygen (11). The regulation of antioxidant enzymes including MnSOD plays an important role in the determination of lifespan, suggesting that the gender difference in antioxidant enzymes explains the difference in life expectancy between females and males.

In the present study we generated a homologous murine model similar to the *daf-2* mutant ($Ir^{P1195L/wt}$) mouse in order to investigate the biological significance of longevity mutations found in the *daf-2* gene of *C. elegans*. We demonstrated that the mutant mice acquired an enhanced resistance to oxidative stress. Furthermore, we also revealed that the influence of gender difference and dietary restriction (DR) on the acquired resistance involved defective insulin signaling.

EXPERIMENTAL PROCEDURES

Generation of Insulin Receptor (IR) Mutant Mice—The 129 mouse genomic library in λFIXII (Stratagene, La Jolla, CA) was screened with rat IR cDNA containing exon 19–21 as a probe. Three overlapping clones covered exon 15–22 of the mouse IR gene. The 1.1-kb fragment containing exon 20 of the gene was PCR-amplified with two SpeI-anchored primers (5′-GGA CTA GTA GCA TTG AGA ACT GGA-3′ and 5′-GGA CTA GTA CCT GAG TTC AAT GCC A-3′). The SpeI-restricted fragment carrying exon 20 was mutagenized with a 19-bp mutagenic oligonucleotide (5′-GGA TGT CAC TCG AGT CCC T-3′) using the pALTER system (Promega, Madison, WI). The introduced mutation, P1195L, was confirmed present by sequencing. The 2.6-kb short 3′ homologous fragment was amplified with a XhoI-anchored primer (5′-CCG CTC GAG ATA GAG ACT ATT GTA CG-3′) and an ApaI/NotI-anchored primer (5′-ATG GGC CCG CGG CCG CTG TGA ACA TAC CTC TG-3′). XhoI/ApaI-restricted short 3′ homologous fragments were inserted into a XhoI/ApaI-restricted pBluescript II SK (pBSII SK, Stratagene) vector. The 1.3-kb MC1neo cassette flanked by the *lox*p sequence was PCR-amplified from a pMC1neo-lox vector (12) with a SalI-anchored primer (5′-CGC GTC GAC ATA ACT TCG TAT AAT G-3′) and a SalI/EcoRI-anchored primer (5′-CGC GTC GAC GAA TTC ATC GAT ACC GGC GAC ATA-3′). The SalI-restricted MC1neo-*lox*p cassette was inserted into a XhoI-restricted pBSII SK vector containing the short 3′ homologous fragment. The SmaI/SalI-restricted fragment including a mutagenized exon 20 was inserted into a SmaI/SalI-restricted pBSII SK vector containing a short 3′ homologous fragment and a MC1neo-*lox*p cassette. The 7.3-kb-long 5′ homologous fragment was PCR-amplified with a NotI-anchored primer (5′-ATT TGC GGC CGC TGG CTA ACA ACT GAC TC-3′) and an SmaI-anchored primer (5′-TCC CCC GGG TTT CTT GAG ACG AGC-3′). The NotI/SmaI-restricted long 5′ homologous fragment was inserted into a NotI/SmaI-restricted pMC1DT-A (Oriental Yeast, Tokyo, Japan). The resulting construct encompassing the fragment carrying a modified exon 20, the MC1neo-*lox*p cassette, and the short 3′ homologous fragment was restricted with NotI, blunted, and inserted into SmaI-restricted pMC1DT-A containing the long 5′ homologous fragment. The vector was then linearized with NotI and used for the electroporation of embryonic stem cells. Genomic DNAs from 240 G418-resistant embryonic stem clones were screened for homologous recombination by Southern blotting. One embryonic stem clone with the expected homologous recombination was used for generating chimeric mice by the aggregation method as described (13). The chimeric mice were cross-bred with C57BL/6CrSlc (Nihon SLC), and the germline transmission was confirmed by PCR amplification with the primers 5′-GCA TGT ATG TGG ACA CT-3′ and 5′-GTG GAG GTC ATG GTT GAG CA-3′ in agouti offspring. To analyze the sequence of the mutated allele in IR mutant mice, we prepared IR transcripts containing exons 19–21 from livers of homozygous embryos by reverse transcription (RT)-PCR using as primers 5′-GCG AAT TCA ATA ACC CAG GCC GCC CT-3′ and 5′-AGT CTC TCT GGA CAG TTA TCA-3′, as described below. We confirmed the presence of the introduced mutation, P1195L, and the absence of additional mutations in exon 20 of the transcripts by sequencing. To delete the neomycin resistance gene from the germline, we cross-bred heterozygous mice with CAG-Cre mice (kindly provided by Dr. Miyazaki, Osaka University) (14).

Animals were housed in specific pathogen-free facilities on a 12-h light/dark cycle (0800 on, 2000 off) and were fed a standard rodent chow (mouse diet CRF-1, Oriental Yeast, Tokyo) and water *ad libitum* (AL). All protocols for animal use and experiments were reviewed and approved by the Animal Care Committee of the Tokyo Metropolitan Institute of Gerontology.

Southern Blotting and PCR Analysis—For the knock-in allele, genomic DNA was digested with EcoRV, subjected to electrophoresis on a 0.7% agarose gel, and then transferred to a Hybond-N^+ nylon membrane (Amersham Biosciences). Probes were labeled with [α-^{32}P]dCTP (6000 Ci/mmol, Amersham Biosciences) using the Megaprime DNA labeling system (Amersham Biosciences). Membranes were hybridized with a HincII/HincII fragment as a 3′ probe, and the fragment was visualized using a Bioimage analyzer BAS-1000 (Fuji Film, Tokyo, Japan). To differentiate wild-type and mutated alleles, we amplified the genomic fragment harboring exons 20 and 21 by PCR with a sense primer (P1, 5′-GGA ATG ACA AGG GAC ATC TA-3′) and antisense primer (P2, 5′-CAC CTG TTC ATT AGA CAG GCC-3′). PCR products were then digested with EcoRI to separate wild-type and mutated alleles.

Tyrosine Kinase Assay of IR—Livers from day1 neonates were solubilized in 1% Triton X-100, 50 mM HEPES (pH 7.6), 150 mM NaCl, 10 μg/ml leupeptin, 10 μg/ml pepstatin, and 1 mM phenylmethylsulfonyl fluoride. The insoluble material was separated by ultracentrifugation at 100,000 × *g* for 1 h at 4 °C. The supernatant was applied to a wheat germ lectin-agarose column pre-equilibrated with buffer A containing 0.1% Triton X-100, 50 mM HEPES (pH 7.6), 150 mM NaCl, and protease inhibitors. The column was extensively washed using buffer A, and the bound glycoproteins, such as IR, were eluted in buffer A containing 0.3 M *N*-acetylglucosamine. Aliquots of eluate were incubated in the absence or presence of 0.1 nM insulin (Eli Lilly) for 1 h at room temperature. Thereafter, phosphorylation was initiated by the addition of 0.1 mCi of [γ-^{32}P]ATP in the presence of 0.1 nM ATP. After 20 min at room temperature, the reaction was stopped by the addition of stopping solution containing 0.1 M NaF, 4 mM $NaVO_3$, 1 mM EDTA, and 1 mM sodium pyrophosphate. Samples were immunoprecipitated with anti-IR antibody (kindly provided by Dr. Ebina, Tokushima University) (15) and protein A-Sepharose CL-4B (Amersham Biosciences). Labeled phosphoproteins were separated on sodium dodecyl sulfate, 10% polyacrylamide gels and detected by autoradiography.

Measurement of Protein Kinase B Phosphorylation—Mice were injected intravenously with 0.75 units kg^{-1} insulin or equal volume of vehicle. All tissues were collected in liquid nitrogen 5 min after the injection. Frozen tissues were homogenized with 6 (for muscle) or 10 (for liver and kidney) times the volume of the tissue in homogenization buffer (1% Triton X, 50 mM HEPES, pH 7.4, 100 mM sodium pyrophosphate, 100 mM NaF, 10 mM EDTA, 10 mM $NaVO_3$, and 2 mM phenylmethylsulfonyl fluoride). Phosphorylation at Ser-473 of protein kinase B in tissue extracts was analyzed with anti-phosphoprotein kinase B Ser-473 and anti-protein kinase B antibodies (Cell Signaling) as described (16).

Oxidative Stress—Twenty (4-month-old) mice were continuously exposed to 80% oxygen for 14 days in a chamber (50 × 30 × 30 cm). The concentration of fractional inspired O_2 in the chamber was monitored with an oxygen analyzer (G-101-Y, Iijima Products, Gamagouri, Japan) and maintained with a constant flow of 80% oxygen gas (3 liters/min). Exposure was continuous for the time indicated except for a few minutes when the chamber was opened for housekeeping purposes weekly. The mice were fed food and water *ad libitum* and kept on a 12-h dark-light cycle at 25 °C. We checked the survival of mice every 12 h. As chemical oxidative stress, the mice (4-month-old) were intraperitoneally injected with paraquat (Sigma) prepared in phosphate-buffered saline at a dose of 70 mg/kg of body weight. We checked the survival of mice every 2 h until 120 h after the injection.

Analytical Procedures—Blood glucose levels were determined in fed mice (3, 6, and 12 months old) using an automatic monitor, Gluco-card (Hoechst Marion Roussel). Serum insulin levels were measured in 16-week-old mice. Serum obtained from fed mice was analyzed for insulin using a mouse insulin enzyme-linked immunosorbent assay kit (Shibayagi, Japan). In glucose tolerance tests fasting (4-month-old) mice were injected intraperitoneally with 2 g/kg body weight of 20% D-glucose. Blood glucose values were determined in whole blood obtained from the tail at 0, 15, 30, 60, and 120 min after the glucose injection. In insulin tolerance tests, 4-month-old mice were injected intraperitoneally with 1 units/kg of body weight of insulin. Blood glucose values were measured at 0, 15, 30, and 60 min after the injection.

SOD Activity Assay—Livers were homogenized in phosphate-buffered saline, pH 7.4, containing 2 mM EDTA, 2 mM EGTA, 2 mM phenylmethylsulfonyl fluoride, and 4 μg/ml leupeptin, then sonicated 10 times using the handy sonicator. The lysates were spun at 15,000 × *g* for 30 min to remove cell debris. SOD activity was measured by a competitive assay as described previously (17). The amount of protein that inhibits the tetrazolium dye WST-1 (Dojindo, Kumamoto, Japan) reduction to 50% of maximum is defined as 1 unit of SOD activity. Enzymatic activity was expressed in units per mg of protein. To measure MnSOD activity, KCN was added to tissue lysates at a final concentration of 1 mM to inhibit the cupper/zinc (Cu/Zn) SOD activity.

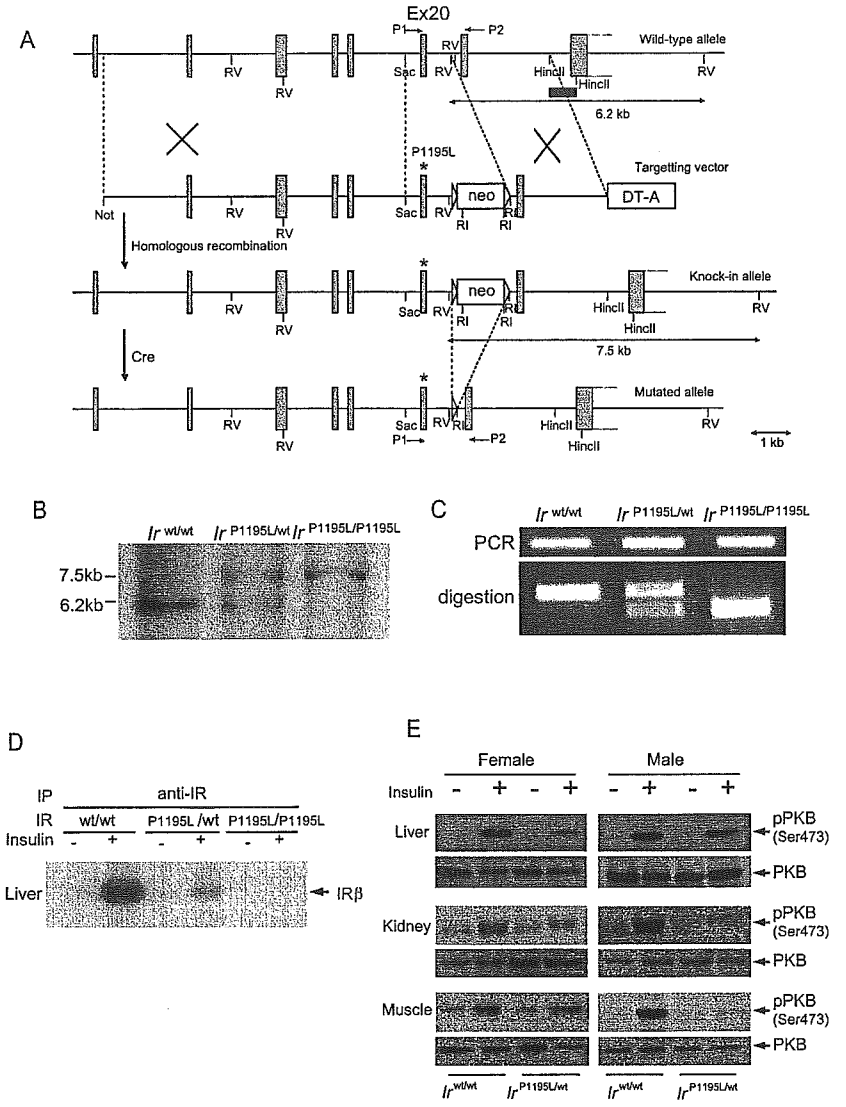

FIG. 1. **Generation of IR mutant mice.** *A*, strategy used to knock-in the IR mutation (P1195L) in the murine IR gene locus. Diagrams of the murine IR genome locus, targeting vector, knock-in allele, and mutated allele are presented. The *open boxes* indicate the neomycin resistance cassette (*neo*) and DT-A gene. Exons are indicated as *solid boxes*. *Open triangles* represent *lox*p sequences. After the cross-breeding with Cre-expressing transgenic mice, the neo cassette was popped out from the genome (mutated allele). The probe for Southern blotting is shown as a *black box*. The *arrows* indicate primers P1 and P2 for PCR. *RI*, EcoRI; *RV*, EcoRV. *B*, Southern blot analysis of EcoRV-digested liver DNAs in embryos. The knock-in allele yielded a 7.5-kbp EcoRV fragment, whereas the wild-type allele yielded a 6.2-kbp EcoRV fragment. *C*, PCR-based genotyping of $Ir^{wt/wt}$, $Ir^{P1195L/wt}$, and $Ir^{P1195L/P1195L}$ embryos. Products amplified with primers P1 and P2 were digested by EcoRI to identify wild-type and mutated alleles. *D*, insulin-induced IR phosphorylation in liver of IR mutant mice. *E*, insulin-induced protein kinase B (*PKB*) phosphorylation in liver, kidney, and muscle of IR mutant mice.

Reverse Transcription (RT)-PCR—Tissues were homogenized in Trizol reagent (Invitrogen). Total RNA was extracted according to the manufacturer's instructions. cDNA was synthesized by reverse transcriptase from 1 μg of total RNA using a RNA PCR kit (Takara Bio Inc., Japan). Mouse MnSOD, Cu/ZnSOD, and glyceraldehyde-3-phosphate dehydrogenase cDNAs were amplified using specific oligonucleotide primers (MnSOD, 5′-GAC CTG CCT TAC GAC TAT GG-3′ and 5′-GAC CTT GCT CCT TAT TGA AGC-3′; Cu/ZnSOD, 5′-ATG AAA GCG GTG TGC GTG CTG-3′ and 5′-AAT CAC TCC ACA GGC CAA GCG-3′; glyceraldehyde-3-phosphate dehydrogenase, 5′-TCG GTG TGA ACG GAT TTG GC-3′ and 5′-ATT TCT CGT GGT TCA CAC CC-3′). PCR products were electrophoresed and visualized using ethidium bromide.

Ovariectomy (OVX) and Estradiol (E2) Administration—At 12 weeks of age, female mice were ovariectomized or sham-operated via a midline incision under anesthesia with pentobarbital (40 mg/kg, intraperitoneal injection). After 4 weeks, treated mice were exposed to 80% oxygen or SOD activity, and gene expression levels were analyzed. Male (12-week-old) mice and OVX female (16-week-old) mice were administered a weekly subcutaneous injection of 17β-estradiol (20 mg/kg per week; Sigma) in corn oil (Ajinomoto, Japan). After 4 weeks of treatment, the male and female mice were exposed to 80% oxygen. E2-treated male mice were analyzed for SOD activity and gene expression.

DR—At 16 weeks of age we measured food intake per day in male and female mice and randomly assigned the mice to two groups, AL and DR. Four mice were housed in every cage (20 × 10 × 20 cm). The mice in the AL group were fed freely, whereas those in the DR group were fed a restricted diet on Monday, Wednesday, and Friday. First, DR mice were fed a 10%-restricted diet for a week, and then the restricted diet was gradually reduced by 65% for 3 weeks. Finally, DR consisted of 65% of food intake in AL mice. We adjusted the amount of restricted diet by measuring food intake in AL mice every 10 weeks. We housed DR mice until the age of 60 weeks.

RESULTS

The Generation of Modified IR Mutant Mice—To elucidate the biological significance of the longevity mutation found in the *daf-2* mutant of *C. elegans*, we generated a homologous murine model by replacing Pro-1195 of IR with Leu by targeted knock-in of the genomic IR gene in mice. As shown in Fig. 1*A*, we first isolated an ES cell carrying a mutation homologous to *daf-2* (*e1391*) (3), *i.e.* Leu-1195 in exon 20 of the IR genomic gene by homologous recombination with the target vector. Germline transmission was confirmed in the F1 offspring of the chimeric and C57BLACK/6 mice by Southern blotting. As shown in Fig. 1*B*, the blot showed that the 3′ probe detected a 6.2-kb polymorphic EcoRV allele in wild-type ($Ir^{wt/wt}$) as well as heterozygous ($Ir^{P1195L/wt}$) mice, whereas the probe detected a 7.5-kb mutant EcoRV allele in heterozygous and homozygous ($Ir^{P1195L/P1195L}$) mice. To delete the neomycin resistance gene from the germline, we cross-bred $Ir^{P1195L/wt}$ mice with CAG-Cre mice (14). We successfully deleted the neomycin resistance gene from the germline by cross-breeding CAG-Cre mice as schematized in the *bottom* of Fig. 1*A*. To detect the wild-type and mutant alleles, we amplified the genomic fragment harboring exon 20 and 21 by PCR with a sense primer (P1) and an antisense primer (P2). The PCR products were then differentiated based on the EcoRI site that is specifically introduced with

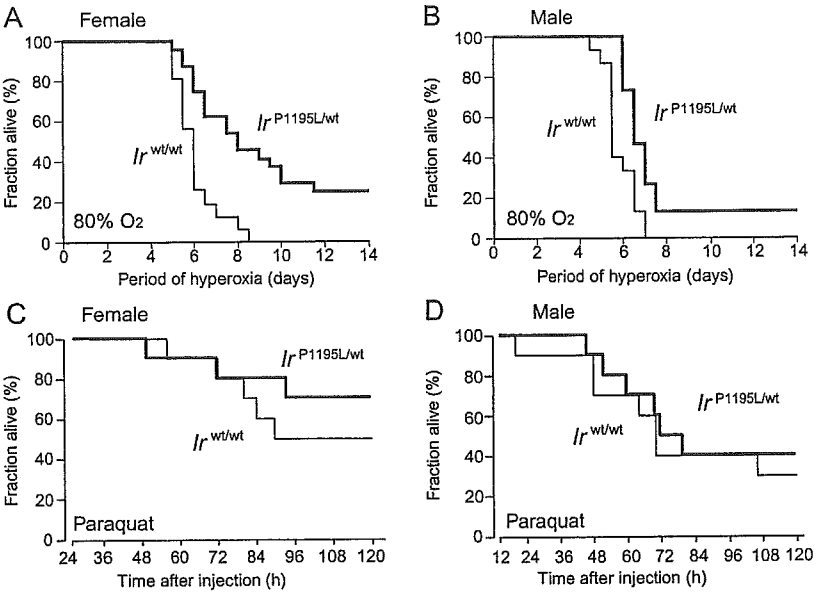

FIG. 2. **IR mutant mice at 4 months of age show resistance to oxidative stress.** *A* and *B*, oxidative stress was induced by exposure to 80% oxygen. Kaplan-Meier analysis showed a significant increase in survival of $Ir^{P1195L/wt}$ compared with $Ir^{wt/wt}$ mice. Female mutants exhibited increased stress resistance ($p < 0.005$, g-Wilcoxon test, at least 16 mice per genotype), whereas male mutants showed a significant increase ($p < 0.05$, g-Wilcoxon test, at least 15 mice per genotype). *C* and *D*, paraquat was injected. $Ir^{P1195L/wt}$ female mice survived longer than wild-type mice beyond 72 h. IR mutant male mice also survived longer than wild-type mice (not significant, g-Wilcoxon test, $n = 10$ in each group).

the knock-in allele (Fig. 1*C*). A genotypic analysis of the offspring showed that the frequency of wild-type, heterozygous and homozygous mice was 31:61:0 at the 4-week-old stage. Further observation, however, showed that some mice were identified as homozygous at 1 day old, which apparently showed that the growth retardation was complicated by the diabetic ketoacidosis.[2] The result suggested that the homozygous mice failed to thrive due to diabetic ketoacidosis in the neonatal stage, which is consistent with the phenotypes previously reported in IR-deficient mice (18, 19).

To investigate the autophosphorylation activity of IR in IR mutant mice, insulin was added to extracts from the neonatal liver of the mice. As shown in Fig. 1*D*, we did not detect any insulin-induced autophosphorylation activity in the $Ir^{P1195L/P1195L}$ mouse. On the other hand, the $Ir^{P1195L/wt}$ mouse did show the insulin-induced autophosphorylation although it was less than 20% that of the $Ir^{wt/wt}$ mouse. Furthermore, to investigate whether the downstream activity of IR is suppressed by the mutation of the IR gene, we monitored protein kinase B phosphorylation, a more distal event in IR signaling (Fig. 1*E*). As with IR autophosphorylation in $Ir^{P1195L/wt}$ mice, insulin-induced protein kinase B phosphorylation was suppressed in liver, kidney, and muscle of $Ir^{P1195L/wt}$ mice compared with $Ir^{wt/wt}$ mice (Fig. 1*E*). These results indicated that the tyrosine kinase activity of IR from heterozygous ($Ir^{P1195L/wt}$) mice was severely suppressed in a dominant negative manner, suggesting that IR mutant mice provide an excellent model for the analysis of longevity phenotypes induced by suppressed insulin signaling compared with heterozygous IR-deficient mice with a haploinsufficiency of insulin signal.

IR Mutant Mice Showed Enhanced Resistance to Oxidative Stress—To investigate whether IR mutant mice acquired enhanced resistance to oxidative stress, the mice at 4 months of age were exposed to 80% oxygen in a chamber. We then compared the survival of IR mutant mice to that of wild-type mice (Fig. 2). IR mutant females survived 33.3% longer than female wild-type mice, *i.e.* IR mutant mice had a 50% survival rate at 8 days compared with 6 days for wild-type mice (Fig. 2*A*). On the other hand IR male mutant mice survived 18.2% longer than wild-type male mice, *i.e.* IR mutant mice had a 50% survival rate at 6.5 days compared with 5.5 days for wild-type mice (Fig. 2*B*). These results suggested that IR mutant mice are more resistant to oxidative stress, but the benefit of the mutation was more pronounced in female than male mice.

Next, we intraperitoneally injected paraquat, a chemical oxidant, into female and male mice to evaluate the defense system of the mutant mice against chemically induced oxidative stress. As shown in Fig. 2*C*, both IR mutant and wild-type female mice began to die ~48 h after the administration of paraquat. IR mutant female mice, however, survived significantly longer than wild-type mice in stages beyond 72 h. IR mutant male mice also survived longer than wild-type mice, but the beneficial effects in male mutant mice were less pronounced in comparison to those in female mutant mice (Fig. 2*D*). These results suggested that IR mutant mice of both genders survived longer than wild-type mice in oxidative conditions. It is also of note that there is a gender difference in the resistance to oxidative stress in IR mutant mice. This data suggested that the insulin signaling may be modulated by sex hormones (*i.e.* either by the beneficial effects of estrogen or by the deleterious effects of testosterone).

MnSOD Plays a Role in the Acquisition of Resistance to Oxidative Stress—Because MnSOD and Cu/ZnSOD play an important role in the intracellular defense against reactive oxygen species (ROS), we measured SOD activities in the liver of IR mutant mice. As shown in Fig. 3*A*, the MnSOD activity of IR mutant female mice was significantly up-regulated by 39.9% compared with that of wild-type female mice (484.9 ± 96.1 units/mg of protein for IR mutant mice *versus* 346.5 ± 51.7 units/mg of protein for wild-type mice, $p < 0.05$). As for male mutant mice, MnSOD activity was up-regulated by 22.9% in comparison with that of wild-type male mice, but the up-regulation was less significant than that found in wild-type female mice (Fig. 3*B*). In contrast, we did not detect any pronounced difference in Cu/ZnSOD activity between IR mutant and wild-type mice of either sex (Fig. 3, *C* and *D*). To analyze the molecular basis for the up-regulation of MnSOD, mRNAs for MnSOD and Cu/ZnSOD were analyzed by RT-PCR (Fig. 3*E*). We found that the transcription of MnSOD was up-regulated in liver, brain, kidney, and heart of both female and male mutant mice, whereas that of the Cu/ZnSOD and glyceraldehyde-3-phosphate dehydrogenase genes was not up-regulated in mutant or wild-type mice (Fig. 3*E*). Furthermore, to investigate the contribution of other antioxidant enzymes to resistance to oxidative stress, we measured activities of glutathione peroxi-

[2] T. Baba, T. Shimizu, Y. Suzuki, H. Koseki, and T. Shirasawa, manuscript in preparation.

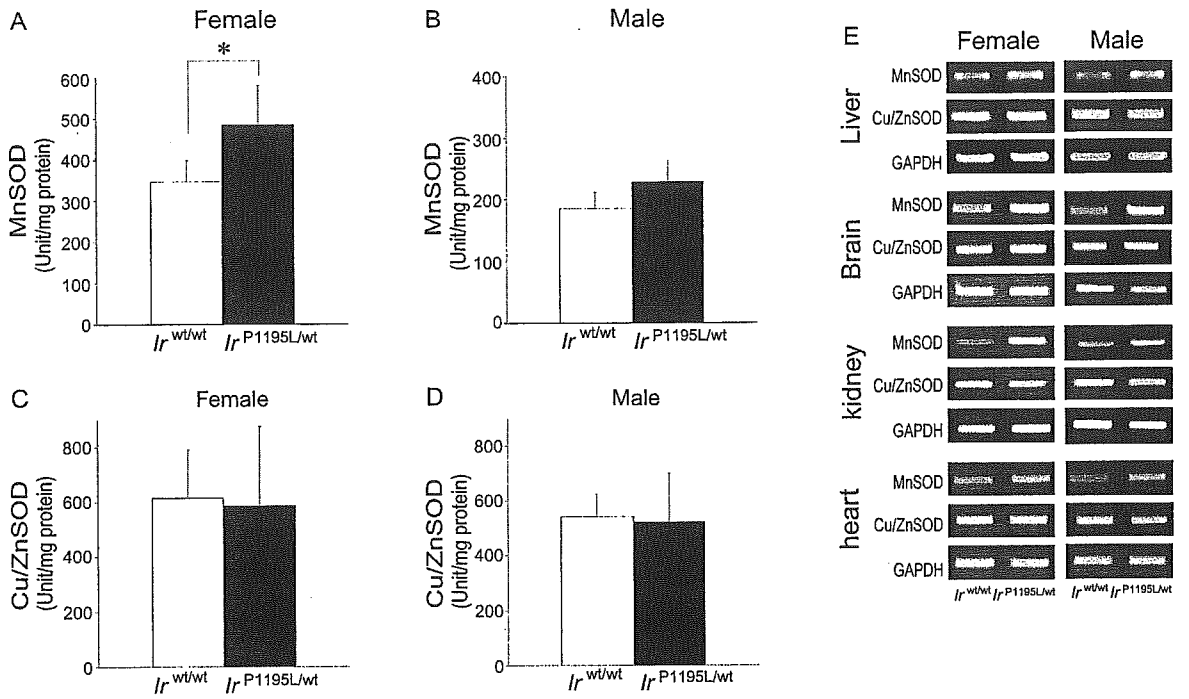

FIG. 3. **The expression and activities of antioxidant enzymes.** *A*, MnSOD activity was significantly stronger in $Ir^{P1195L/wt}$ female mice than $Ir^{wt/wt}$ female mice. *B*, $Ir^{P1195L/wt}$ male mice showed higher levels of MnSOD activity than $Ir^{wt/wt}$ male mice but not significantly so. *C* and *D*, Cu/ZnSOD activity was not up-regulated in mutant mice. *E*, RT-PCR analysis. Expression of the MnSOD gene was stronger in liver, brain, kidney, and heart of $Ir^{P1195L/wt}$ male and female mice than $Ir^{wt/wt}$ mice. Expression of the Cu/ZnSOD gene was not up-regulated in mutant mice. The glyceraldehyde-3-phosphate dehydrogenase (*GAPDH*) gene as an internal control is shown. Each *bar* represents the mean ± S.D. in each group from at least five mice per genotype. *, $p < 0.05$; $Ir^{P1195L/wt}$ mice *versus* $Ir^{wt/wt}$ mice.

dase and catalase. However, we did not detect any significant differences between IR mutant and wild-type mice (data not shown). These results suggested that the transcriptional up-regulation of MnSOD is specific to the enhanced antioxidant system in IR mutant mice. In *C. elegans* and *Drosophila melanogaster*, the up-regulated SODs are reported to degrade the oxygen radicals that cause oxidative stress in IR/ IGF-1 receptor mutants (5, 6, 20). Kops *et al.* (21) reported that MnSOD was up-regulated upon treatment with insulin in cultured 3T3-L6 cells. Here we demonstrated for the first time that the expression and the activity of MnSOD were up-regulated by the mutation introduced into the kinase domain of the IR gene in mice. Transgenic flies, which overexpressed Cu/ZnSOD in motor neurons, survived 40% longer than control fruit flies, whereas transgenic flies that overexpressed MnSOD in motor neurons survived 30% longer than control flies (22, 23). The up-regulation of MnSOD may confer an extension of lifespan in *Drosophila*. The regulation of MnSOD by insulin signaling was shown to be conserved between invertebrates and mammals, suggesting that the antioxidant system against ROS plays an important role in the determination of animal lifespan in both invertebrates and vertebrates.

Estrogen Signaling Enhances Tolerance to Oxidative Stress in IR Mutant Mice—The MnSOD activity of female mice was significantly up-regulated in comparison with that of male mice (Fig. 3, *A* and *B*). Strehlow *et al.* (24) reported that the gene expression of MnSOD and extracellular SOD in ovariectomized mice was down-regulated to 40–60% that of the control level and was recovered through estrogen replacement therapy (24). To investigate whether estrogen signaling confers resistance to oxidative stress and up-regulates MnSOD expression in IR mutant mice, we performed OVXs on female mice. For male mice, on the other hand, we administered E2 for 4 weeks.

First, we investigated the oxidative tolerance under hyperoxic conditions and the activity of MnSOD in the liver of OVX mice. As shown in Fig. 4, *A* and *B*, we compared the survival rate of OVX mice with that of non-OVX mice in both the IR mutant mice and wild-type strains. OVX mutant mice died significantly earlier than non-OVX mutant mice, *i.e.* OVX mutant mice had a 50% survival rate at 6.5 days compared with 12 days for non-OVX mutant mice (Fig. 4*A*). OVX wild-type mice died earlier than non-OVX wild-type mice, *i.e.* OVX wild-type mice had a 50% survival rate at 5.5 days compared with 7 days for non-OVX wild-type mice (Fig. 4*B*). The shortening of the survival rate was more pronounced in IR mutant mice than the wild-type mice, when both were ovariectomized. To clarify the molecular mechanisms of shortened survival in OVX mice, we investigated the gene expression and enzyme activity of MnSOD in the liver of mutant mice. As shown in Fig. 5*A*, the MnSOD activity of IR mutant mice was significantly down-regulated upon OVX (484.9 ± 96.1 units/mg of protein for mutant mice *versus* 387.3 ± 88.9 units/mg of protein for OVX mutant mice, $p < 0.05$). The down-regulation of MnSOD activity was less pronounced in wild-type OVX mice. In contrast, we did not detect any difference in Cu/ZnSOD activity upon OVX (Fig. 5*C*). The transcription of MnSOD was significantly down-regulated in OVX mice (Fig. 5*E*).

Second, to investigate the influence of exogenous estrogen on male mice, we administered E2. After exposure to 80% oxygen, we compared the survival of males treated with E2 to that of untreated make of both IR mutant mice and wild-type mice. Interestingly, mutant males administered E2 survived significantly longer than untreated mutant mice (Fig. 4*E*). The extension of survival was more pronounced in IR mutant mice than wild-type mice, when both were administered estrogen (Fig. 4, *E* and *F*). As shown in Fig. 5*B*, MnSOD activity was up-regulated by 20.6% in IR mutant mice treated with E2. The MnSOD activity of wild-type male mice was also up-regulated by 15.3% upon administration of E2. In contrast, we found no up-regulation of Cu/ZnSOD activity with E2 administration. (Fig. 5*D*). The transcription of MnSOD was significantly up-regulated in male mice administered E2 (Fig. 5*F*).

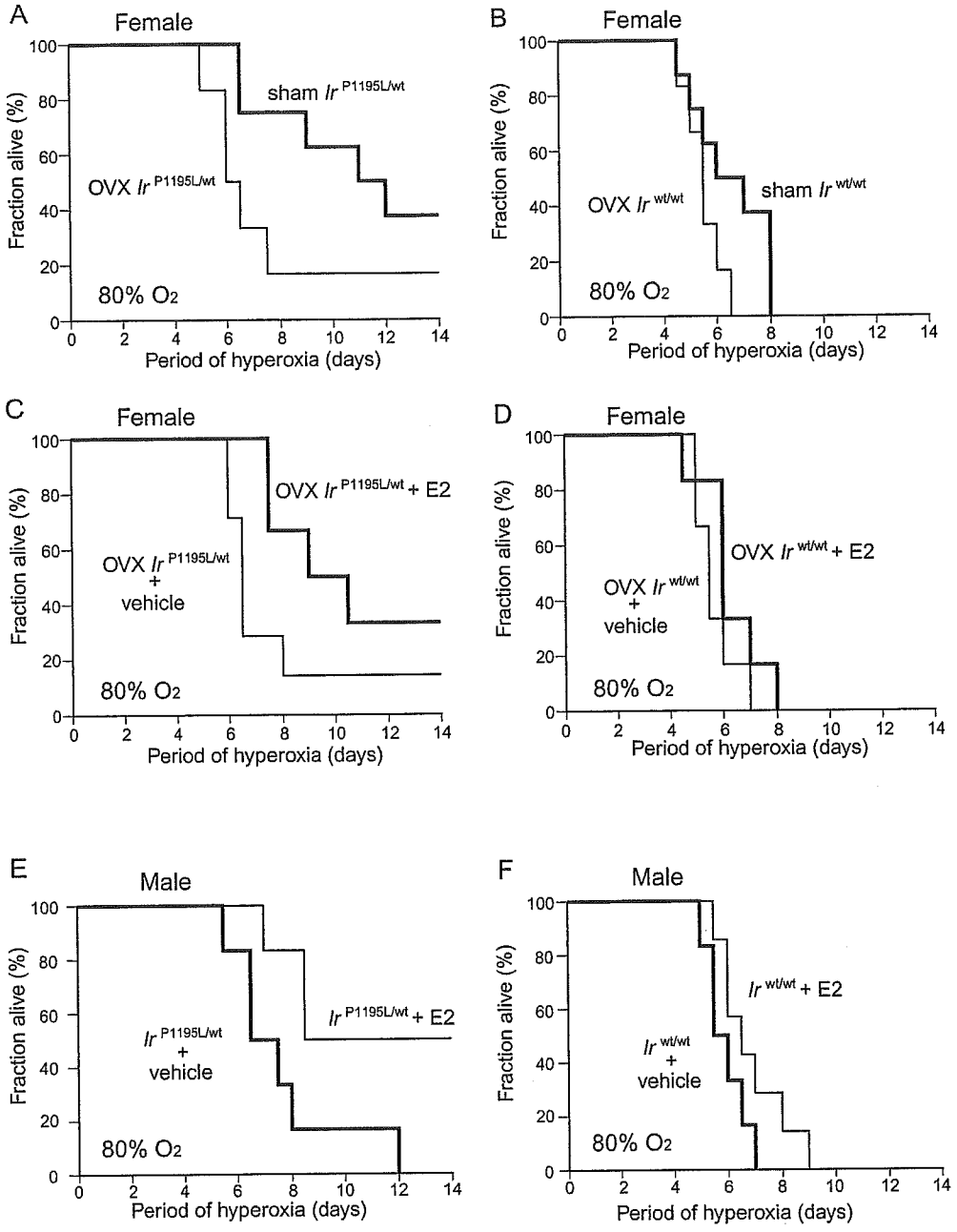

FIG. 4. **Estrogen signaling enhances resistance to oxidative stress in $Ir^{P1195L/wt}$ mice.** *A* and *B*, OVX mice died earlier than non-OVX mice. The shortening of the survival period was greater in $Ir^{P1195L/wt}$ mice ($p < 0.05$, g-Wilcoxon test) than $Ir^{wt/wt}$ mice (not significant, g-Wilcoxon test). *C* and *D*, estrogen replacement improved the resistance to oxidative stress in OVX mice. The influence of E2 was remarkable in $Ir^{P1195L/wt}$ female mice ($p < 0.05$, g-Wilcoxon test) compared with $Ir^{wt/wt}$ mice (not significant, g-Wilcoxon test) upon OVX. *E* and *F*, male mice treated with E2 survived longer than untreated mice. The influence of E2 was remarkable in $Ir^{P1195L/wt}$ male mice ($p < 0.05$, g-Wilcoxon test) compared with $Ir^{wt/wt}$ mice (not significant, g-Wilcoxon test).

Finally, to exclude the possibility that the deficiency of testosterone caused by the feedback regulation of E2 administration is attributable to the phenotype of E2-treated males, we investigated the influence of exogenous estrogen on OVX mice. After 4 weeks of E2 administration, OVX mice were exposed to 80% oxygen. OVX mutant mice treated with E2 survived significantly longer than untreated mutant mice; the E2-treated group had 50% survival at 10.5 days compared with 6.5 days for the untreated group (Fig. 4*C*). OVX wild-type mice treated with E2 also survived longer than untreated wild-type male mice but not significantly so (Fig. 4*D*). We demonstrated here that mutant mice administered E2 survived longer with hyperoxygen as well as showed an up-regulation of MnSOD expression. Interestingly, the influence of estrogen was remarkable on IR mutant mice compared with wild-type mice.

The Gender Difference of Glucose Metabolism in IR Mutant Mice—To determine whether the suppression of IR signaling induces an impairment of glucose metabolism, levels of glucose (Fig. 6*A*) and insulin (Fig. 6*B*) were analyzed in blood samples. In a fed state, IR mutant mice had almost the same blood glucose concentrations as wild-type mice. However, about 6% of mutant male mice developed hyperglycemia (more than 200 mg/dl) (Fig. 6*A*). This rate was the same as in mice heterozygous for insulin receptor knock-out (25). In contrast, we did not detect any differences in urinary glucose between mutant and wild-type mice (data not shown). Serum insulin concentrations in the fed state were significantly increased in both female and male mutant mice compared with wild-type mice (Fig. 6*B*).

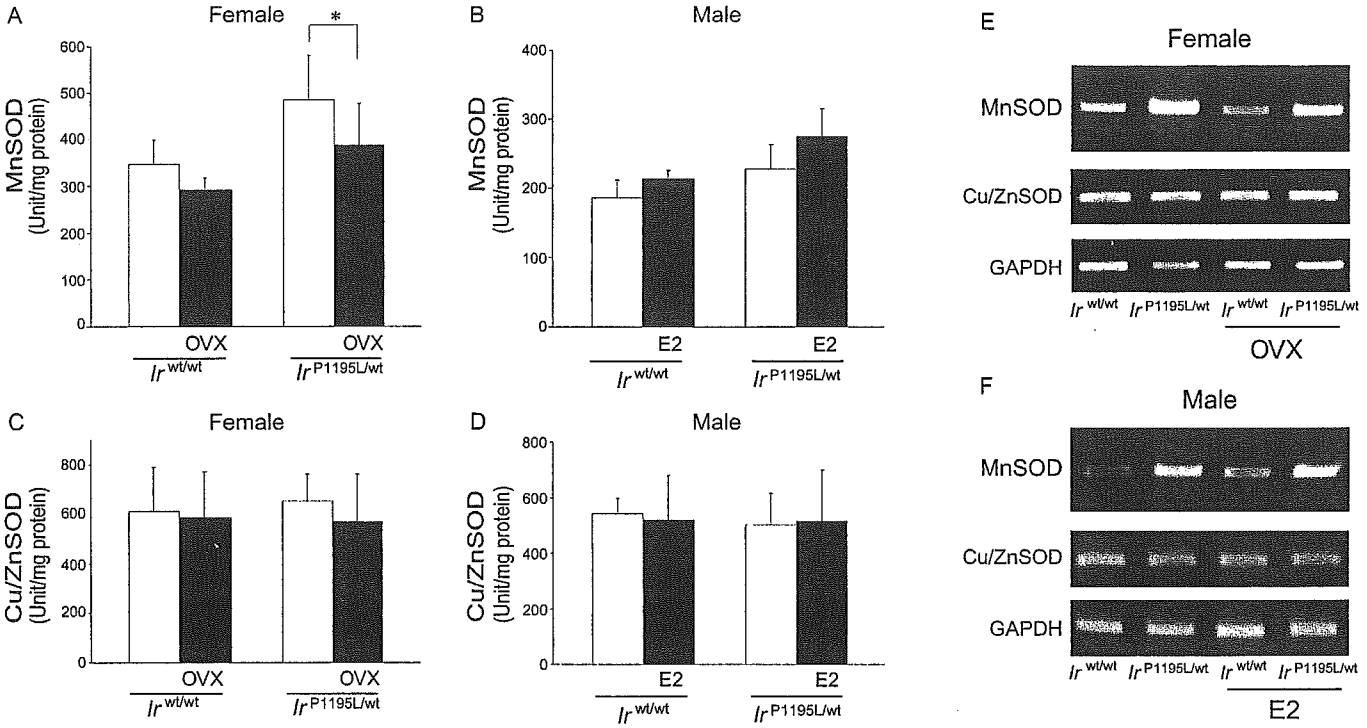

FIG. 5. **Activities and transcriptional expression of antioxidant enzymes.** *A*, MnSOD activity was down-regulated in OVX female mice. *B*, MnSOD activity was up-regulated in male mice when exogenous E2 was administered. *C* and *D*, Cu/ZnSOD activity was not up-regulated in OVX or E2-administered mutant mice. *E* and *F*, MnSOD transcription in the RT-PCR analysis was down-regulated upon OVX in female mice and up-regulated in male mice treated with E2. Each *bar* represents the mean ± S.D. in each group from at least five mice per genotype. *, $p < 0.05$; $Ir^{P1195L/wt}$ mice *versus* $Ir^{wt/wt}$ mice. *GAPDH*, glyceraldehyde-3-phosphate dehydrogenase.

Although we failed to detect any gender difference in insulin concentrations of wild-type mice, insulin concentrations were significantly increased in IR mutant males (6.40 ± 1.49 ng/ml) compared with IR mutant females (2.96 ± 1.63 ng/ml) (Fig. 6*B*).

To determine the physiological consequence of mutated IR, glucose and insulin tolerance tests were performed on 4-month-old mice. Both female and male IR mutant mice showed normal fasting blood glucose concentrations as compared with control mice (Fig. 6, *C* and *D*). However, IR mutant male mice showed a moderately impaired glucose tolerance as compared with control male mice (Fig. 6*D*), whereas IR mutant female mice showed normal glucose tolerance (Fig. 6*C*). In addition, IR mutant females were more sensitive to blood glucose-lowering effects than wild-type mice when insulin was administered (Fig. 6*E*). In contrast, IR mutant male mice showed resistance to blood glucose-lowering effects in the insulin tolerance test (Fig. 6*F*). Although IR signaling was suppressed in IR mutant mice, mutant females sustained insulin sensitivity with hyperinsulinemia. This gender difference suggested that sex hormones may modulate the insulin signaling in IR mutant mice.

Then, to investigate whether sex hormones influence glucose metabolism, glucose and insulin tolerance tests were performed on female OVX mice and male mice treated with E2. Upon OVX, the glucose tolerance of IR mutant mice showed no significant changes as compared with that of wild-type mice (Fig. 6*G*). However, OVX mutant mice showed impaired insulin sensitivity compared with non-OVX mutant mice (Fig. 6, *E* and *I*). Furthermore, E2 administration improved glucose intolerance and insulin resistance in IR mutant male mice (Fig. 6, *H* and *J* compared with *D* and *F*). In contrast, wild-type mice showed no significant changes upon the administration of E2.

As for the mechanism of action of estrogen, Pedersen *et al.* (26) reported that IR binding was increased in adipocytes from rodents treated with estrogen. In that case, IR binding seemed to be due to an increased number of IRs (26). Yu *et al.* (27) reported that an IR signaling pathway is involved in estrogen-mediated retinal neuroprotection. The influence of estrogen is remarkable on IR mutant mice when compared with wild-type mice, suggesting that estrogen partially enhances its effect through insulin signaling.

DR Additively Enhances the Resistance against Oxidative Stress in IR Mutant Mice—Dietary restrictions that facilitate a reduction in body weight, mainly fat mass, are known to prolong lifespan by enhancing resistance against oxidative stress in mammals (28–30). Bluher *et al.* reported that fat-specific insulin receptor knock-out mice showed reduced adiposity, suggesting that the reduction of fat mass may be beneficial for the extension of lifespan (31, 32). To clarify whether there is a reduction of adipose tissue induced by mutation in the IR gene, we observed whole body and organ weights of IR mutant mice. Both male and female IR mutant mice sustained a significant 10–15% reduction in body weight compared with wild-type mice (Fig. 6, *A* and *B*). The fat mass of IR female mutant mice decreased significantly by 41.3% when compared with wild-type mice (446.6 ± 36.1 *versus* 761.4 ± 183.0 mg, $p < 0.05$), whereas that of IR male mutant mice dropped significantly by 57.5% compared with wild-type mice (522.9 ± 54.7 *versus* 1230.0 ± 196.0 mg, $p < 0.01$). We found no difference in the weights of other organs between IR mutant and wild-type mice (Fig. 6, *A* and *B*). To exclude the possibility that IR mutant mice show reduced food intake, we measured the food intake of mice at age of 16 weeks. We did not detect any significance difference in food intake between wild-type and mutant mice (female; 3.37 ± 0.1 *versus* 3.45 ± 0.18 g/day, male; 3.54 ± 0.11 *versus* 3.57 ± 0.15 g/day). We demonstrated that IR mutant mice specifically exhibited a reduction in fat mass, suggesting that the phenotype of IR mutant mice is very similar to that of fat-specific insulin receptor knock-out mice (31, 32).

To elucidate the influence of DR in IR mutant mice, the diet was restricted to 65% that consumed by the mice fed *ad libi-*

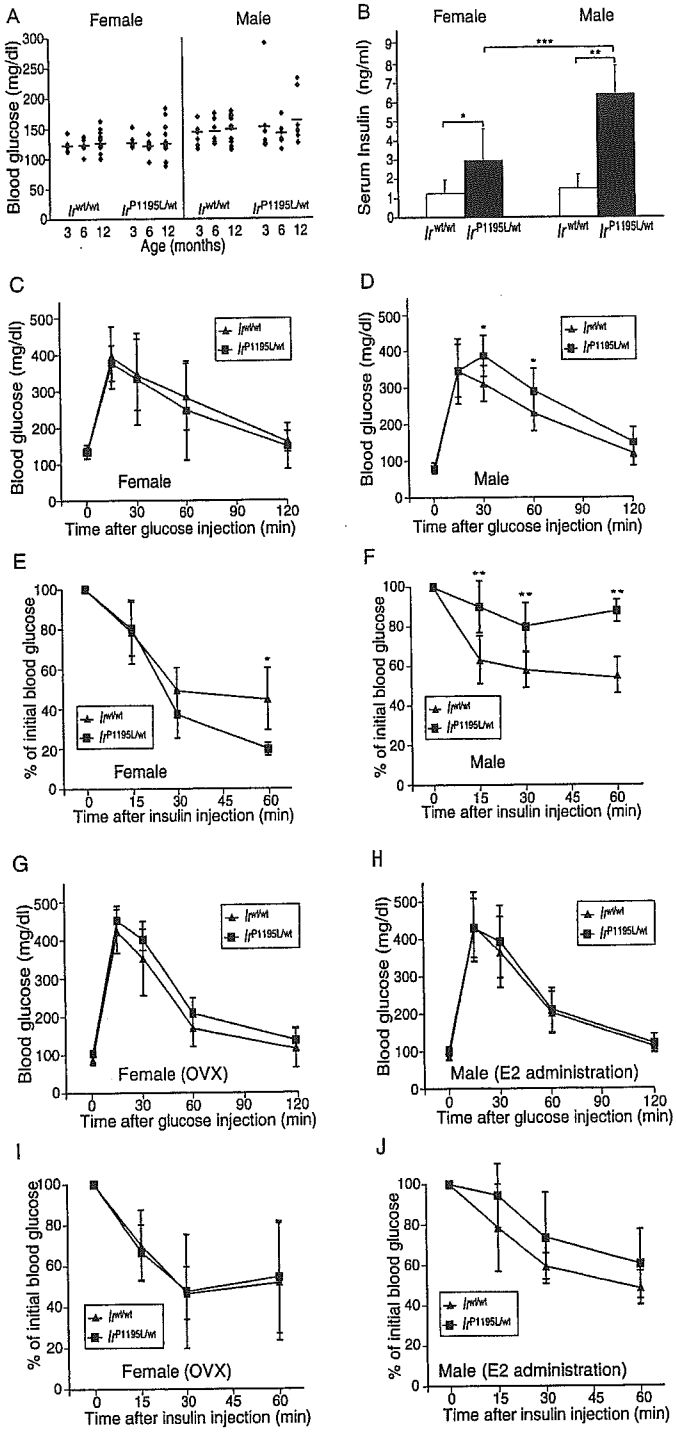

FIG. 6. **The gender difference of glucose metabolism in IR mutant mice.** *A*, most $Ir^{P1195L/wt}$ mice exhibited blood glucose concentrations within the range of $Ir^{wt/wt}$ mice. *B*, insulin concentrations were significantly increased in $Ir^{P1195L/wt}$ male mice as compared with $Ir^{P1195L/wt}$ female mice. *C* and *D*, glucose tolerance tests performed on 4-month-old $Ir^{P1195L/wt}$ mice. We did not detect any differences in glucose tolerance between $Ir^{P1195L/wt}$ and $Ir^{wt/wt}$ female mice (C). $Ir^{P1195L/wt}$ male mice showed moderately impaired glucose tolerance compared with $Ir^{wt/wt}$ male mice (*D*). *E* and *F*, insulin tolerance tests were performed on random-fed, 4-month-old $Ir^{P1195L/wt}$ mice. The testing demonstrated that $Ir^{P1195L/wt}$ female mice were more sensitive to insulin than $Ir^{wt/wt}$ female mice (*E*). $Ir^{P1195L/wt}$ male mice were resistant to insulin (*F*). Upon OVX, glucose tolerance of $Ir^{P1195L/wt}$ mice showed no significant change as compared with that of $Ir^{wt/wt}$ mice (*G*). OVX $Ir^{P1195L/wt}$ mice showed an impaired insulin sensitivity compared with non-OVX mice (*I*). E2 administration improved glucose intolerance and insulin resistance in $Ir^{P1195L/wt}$ male mice (*H* and *J*). Each *bar* represents the mean ± S.D. in each group from at least six mice per genotype. *, $p < 0.05$; **, $p < 0.01$; ***, $p < 0.005$; $Ir^{P1195L/wt}$ mice *versus* $Ir^{wt/wt}$ mice.

tum. As a result, IR mutant female mice with DR showed a 78.9% reduction of fat mass compared with AL wild-type mice, whereas the mutant males with DR showed an 88.4% reduction (Fig. 7, *A* and *B*). Although IR mutant and wild-type mice with DR also showed a reduction in the weights of other tissues, it was not as remarkable as that observed in fat mass. We demonstrated that genetic manipulation further enhances the reduction of fat mass induced by DR.

To clarify the influence of the reduction in fat tissue in IR mutant mice, we exposed IR mutant and wild-type mice to 80% oxygen. Interestingly, IR mutant mice showed a comparable survival rate to wild-type mice with DR (Fig. 7, *C* and *D*). The result suggested that genetic factors as well as DR independently play an important role, although we could not rule out cross talk between them. Surprisingly, IR mutant female and male mice both showed an extended lifespan upon DR (Fig. 7, *C* and *D*). Houthoofd *et al.* (33) reported that lifespan extension via DR is independent of the insulin/IGF-1 signaling pathway in *C. elegans*. Although the reduction of fat mass induced by DR is more pronounced in mutant males than females, IR mutant female mice survived longer than IR mutant male mice under oxidative conditions. These results indicated that IR mutant female mice showed beneficial effects of DR as well as endogenous estrogen for the resistance to oxidative stress.

DISCUSSION

MnSOD Is Up-regulated in Vivo in IR Mutant Mice—Daf-2 is one of the longevity mutants found in *C. elegans* (3). The causative mutation was found in the gene encoding the insulin-like receptor, suggesting that the *daf-2* mutant has a defective insulin-like signaling, which eventually triggers the dauer formation as well as the extension of lifespan in *C. elegans* (3, 4). The mutation of *daf-16*, a major suppressor mutant for *daf-2*, was found in the gene encoding the forkhead transcription factor (34, 35). Biochemical analyses revealed that DAF-16, or dFOXO of the fly ortholog, played a pivotal role as a transcription factor by regulating the longevity genes downstream of the insulin signaling pathway (34–36). The signaling pathway triggered by insulin or insulin-like ligands is well conserved among various animal species, including mammals and invertebrates such as *D. melanogaster*, in which mutants for the insulin receptor, *IR*, or *IRS-1*, *chico*, also exhibit the longevity phenotype (6, 20). One of the candidate longevity genes in the downstream of *daf-16* is the MnSOD gene (37), whose expression is specifically up-regulated in *daf-2* mutants (5). Because biochemical studies show that MnSOD catalyzes the superoxide endogenously generated in the mitochondrial matrix, the balance between the generation of ROS and its degradation capacity in mitochondria may be critical for the determination of lifespan (38), which favors the free radical theory of aging (39, 40). Kops *et al.* (21) recently demonstrated *in vitro* that FOXO3a, a homologue of DAF-16, actually induced the expression of MnSOD, enhancing the antioxidative defense system in cultured mammalian cells challenged with oxidative stress. In the present study we demonstrated for the first time that MnSOD expression is up-regulated *in vivo* by defective insulin signaling in IR mutant mice. Because IR mutant mice carry a mutation homologous with *daf-2* with respect to the severely suppressed signaling of insulin, the up-regulation of MnSOD suggests that one of the longevity signals is sent to the anti-oxidative defense system, which is well conserved between invertebrates and mammals. Although further analyses are needed for elucidation of the molecular basis for the regulation of MnSOD, we found the transcriptional up-regulation of the MnSOD gene in IR mutant mice, suggesting the direct involvement of DAF-16 in the regulation of the mammalian MnSOD gene.

Estrogen Confers Resistance to Oxidative Stress by Up-regulating the MnSOD Gene—As shown in Fig. 4, the acquired

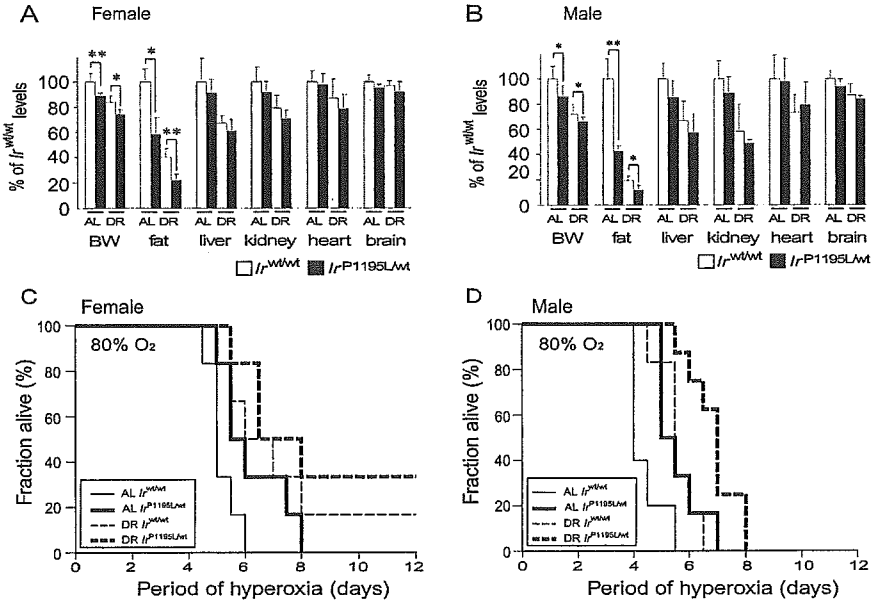

FIG. 7. **The influence of DR in IR mutant mice.** *A* and *B*, comparison of mean body weights (*BW*) and organ weights between $Ir^{P1195L/wt}$ mice and $Ir^{wt/wt}$ mice. $Ir^{P1195L/wt}$ mice had significantly lower body weights than $Ir^{wt/wt}$ mice. The reduction in fat mainly causes the reduction in body weight. *C* and *D*, R additively enhances the resistance against hyperoxygen in $Ir^{P1195L/wt}$ mice. Each *bar* represents the mean ± S.D. in each group from at least five mice per genotype. *, $p < 0.05$; **, $p < 0.01$; $Ir^{P1195L/wt}$ mice *versus* $Ir^{wt/wt}$ mice.

resistance to oxidative stress observed in female IR mutant mice was significantly attenuated when their ovaries were surgically removed. Because the ovary secretes the sex hormones estrogen and progesterone, either or both sex hormones confer resistance to oxidative stress in the mutant mice. To address this endocrinological issue, we administered E2 to male IR mutant mice as well as wild-type littermates. Interestingly, both the mutant and wild-type mice survived longer when they were administered E2, suggesting that estrogen made the male mice resistant to oxidative stress. This result is particularly interesting given that patients with prostate cancer are often prescribed with estradiol for hormone therapy. It is also interesting that female animals including humans generally live longer than males. In this context female hormones may protect the body from oxidative stress during the reproductive period, but the beneficial effects would fade after menopause. These assumptions are highly compatible with the notion that age-associated disease, such as atherosclerosis, osteoporosis, and dementia tend to appear more frequently after menopause in elderly females.

As for the molecular mechanism by which estrogen affects the signaling pathway triggered by insulin, Bailey *et al.* (41) showed that ovariectomized rodents showed an impaired glucose tolerance with an impaired secretion of insulin, suggesting that sex hormones have a direct pharmacological effect on the endocrinological function of insulin. In humans as well, postmenopausal women develop insulin resistance associated with an increase in body fat. Estrogen hormone replacement therapy improves insulin sensitivity with significant loss of fat tissue (42). Because the pharmacological actions of estrogen depend on the receptor subtypes expressed in each tissue, subtype-specific effects of estrogen should be investigated in subtype-specific estrogen receptor (ER)-deficient mice, ERα-deficient or ERβ-deficient mice (43, 44).

DR Confers Distinct Signaling for the Determination of Lifespan—Evidence has accumulated that DR extends the lifespan of animals associated with an enhanced resistance to oxidative stress in various species (28–30). Mutant mice with growth hormone signaling such as Ames dwarf mice showed extended lifespan compared with wild-type mice when they were raised in an ordinary laboratory environment (45–47). Interestingly, these mutant mice had an even longer lifespan when raised with a reduced diet (48). The result suggests that the longevity signaling evoked by DR may be in large part independent and distinct from the insulin signaling, although DR itself suppresses glucose metabolism and insulin secretion because of the restricted dietary intake.

Another genetic model, the fat-specific insulin receptor knock-out mouse, which has a tissue-specific defect of insulin signaling in adipose tissue, showed reduced adiposity without a restriction of diet. These mice also showed extended lifespan even when they were raised with an ordinary diet, suggesting that the reduction in fat mass attributed to the longer lifespan (32). It is, thus, speculated that the amount of fat mass may be a major determinant of lifespan irrespective of environmental factors or genetic factors. In the present study, however, we revealed that the amount of fat mass and the resistance to oxidative stress are not necessarily correlated (Fig. 7, *B* and *D*), suggesting that not only the reduction of fat mass but other environmental or genetic factors contribute to the acquired resistance to oxidative stress. The idea that DR has an independent and distinct signaling mechanism from insulin is also supported by the report that *daf-2* mutants showed additional extension of lifespan in *C. elegans* when their diet of was restricted (33).

In the present study we demonstrated that in IR mutant mice resistance to oxidative stress was further enhanced by DR or E2. We are still finishing an analysis of the lifespan of IR mutant mice under normoxic conditions. We also expect a gender difference in the lifespan of IR mutant mice based on the analysis in oxygen chambers. Female mutant mice may have an enhanced defense system due to the estrogen secreted by the ovaries during the reproductive period. We demonstrated here that three distinct signals, insulin, estrogen, and dietary signals, work in different and independent ways and together increase resistance to oxidative stress and MnSOD levels in mice.

Acknowledgements—We thank Drs. Nakajima, Takahashi, Uchiyama, Moriizumi, Ikegami, Nakai, Huang, Nojiri, Kawakami, Kuwahara, and Sakuramoto for technical assistance. We especially thank Dr. Miyazaki of Osaka University for CAG-Cre transgenic mice, Dr. Ebina of Tokushima University for anti-IR antibody, and Drs. Kojima and Takahashi of Tokyo University of Science for valuable discussions.

REFERENCES

1. Finkel, T., and Holbrook, N. J. (2000) *Nature* **408,** 239–247
2. Martin, G. M., Austad, S. N., and Johnson, T. E. (1996) *Nat. Genet.* **13,** 25–34
3. Kimura, K. D., Tissenbaum, H. A., Liu, Y., and Ruvkun, G. (1997) *Science* **277,** 942–946

4. Kenyon, C., Chang, J., Gensch, E., Rudner, A., and Tabtiang, R. (1993) *Nature* **366,** 461–464
5. Honda, Y., and Honda, S. (1999) *FASEB J.* **13,** 1385–1393
6. Clancy, D. J., Gems, D., Harshman, L. G., Oldham, S., Stocker, H., Hafen, E., Leevers, S. J., and Partridge, L. (2001) *Science* **292,** 104–106
7. Holzenberger, M., Dupont, J., Ducos, B., Leneuve, P., Geloen, A., Even, P. C., Cervera, P., and Le Bouc, Y. (2003) *Nature* **421,** 182–187
8. Smith, D. W. (1989) *Biol. Rev. Camb. Philos. Soc.* **64,** 1–12
9. Borras, C., Sastre, J., Garcia-Sala, D., Lloret, A., Pallardo, F. V., and Vina, J. (2003) *Free Radic. Biol. Med.* **34,** 546–552
10. Ho, Y. S., Vincent, R., Dey, M. S., Slot, J. W., and Crapo, J. D. (1998) *Am. J. Respir. Cell Mol. Biol.* **18,** 538–547
11. Wispe, J. R., Warner, B. B., Clark, J. C., Dey, C. R., Neuman, J., Glasser, S. W., Crapo, J. D., Chang, L. Y., and Whitsett, J. A. (1992) *J. Biol. Chem.* **267,** 23937–23941
12. Taniguchi, M., Sanbo, M., Watanabe, S., Naruse, I., Mishina, M., and Yagi, T. (1998) *Nucleic Acids Res.* **26,** 679–680
13. Nagy, Z. P., Joris, H., Liu, J., Staessen, C., Devroey, P., and Van Steirteghem, A. C. (1993) *Hum. Reprod.* **8,** 2180–2184
14. Sakai, K., and Miyazaki, J. (1997) *Biochem. Biophys. Res. Commun.* **237,** 318–324
15. Imanaka, T., Hayashi, H., Kishi, K., Wang, L., Ishii, K., Hazeki, O., Katada, T., and Ebina, Y. (1998) *J. Biol. Chem.* **273,** 25347–25355
16. Um, S. H., Frigerio, F., Watanabe, M., Picard, F., Joaquin, M., Sticker, M., Fumagalli, S., Allegrini, P. R., Kozma, S. C., Auwerx, J., and Thomas, G. (2004) *Nature* **431,** 200–205
17. Ikegami, T., Suzuki, Y., Shimizu, T., Isono, K., Koseki, H., and Shirasawa, T. (2002) *Biochem. Biophys. Res. Commun.* **296,** 729–736
18. Accili, D., Drago, J., Lee, E. J., Johnson, M. D., Cool, M. H., Salvatore, P., Asico, L. D., Jose, P. A., Taylor, S. I., and Westphal, H. (1996) *Nat. Genet.* **12,** 106–109
19. Joshi, R. L., Lamothe, B., Cordonnier, N., Mesbah, K., Monthioux, E., Jami, J., and Bucchini, D. (1996) *EMBO J.* **15,** 1542–1547
20. Tatar, M., Kopelman, A., Epstein, D., Tu, M. P., Yin, C. M., and Garofalo, R. S. (2001) *Science* **292,** 107–110
21. Kops, G. J., Dansen, T. B., Polderman, P. E., Saarloos, I., Wirtz, K. W., Coffer, P. J., Huang, T. T., Bos, J. L., Medema, R. H., and Burgering, B. M. (2002) *Nature* **419,** 316–321
22. Parkes, T. L., Elia, A. J., Dickinson, D., Hilliker, A. J., Phillips, J. P., and Boulianne, G. L. (1998) *Nat. Genet.* **19,** 171–174
23. Phillips, J. P., Parkes, T. L., and Hilliker, A. J. (2000) *Exp. Gerontol.* **35,** 1157–1164
24. Strehlow, K., Rotter, S., Wassmann, S., Adam, O., Grohe, C., Laufs, K., Bohm, M., and Nickenig, G. (2003) *Circ. Res.* **93,** 170–177
25. Kitamura, T., Kahn, C. R., and Accili, D. (2003) *Annu. Rev. Physiol.* **65,** 313–332
26. Pedersen, S. B., Borglum, J. D., Moller-Pedersen, T., and Richelsen, B. (1992) *Mol. Cell. Endocrinol.* **85,** 13–19
27. Yu, X., Rajala, R. V., McGinnis, J. F., Li, F., Anderson, R. E., Yan, X., Li, S., Elias, R. V., Knapp, R. R., Zhou, X., and Cao, W. (2004) *J. Biol. Chem.* **279,** 13086–13094
28. Hamilton, M. L., Van Remmen, H., Drake, J. A., Yang, H., Guo, Z. M., Kewitt, K., Walter, C. A., and Richardson, A. (2001) *Proc. Natl. Acad. Sci. U. S. A.* **98,** 10469–10474
29. Lee, S. S., and Ruvkun, G. (2002) *Nature* **418,** 287–288
30. Sohal, R. S., and Weindruch, R. (1996) *Science* **273,** 59–63
31. Bluher, M., Michael, M. D., Peroni, O. D., Ueki, K., Carter, N., Kahn, B. B., and Kahn, C. R. (2002) *Dev. Cell* **3,** 25–38
32. Bluher, M., Kahn, B. B., and Kahn, C. R. (2003) *Science* **299,** 572–574
33. Houthoofd, K., Braeckman, B. P., Johnson, T. E., and Vanfleteren, J. R. (2003) *Exp. Gerontol.* **38,** 947–954
34. Lin, K., Dorman, J. B., Rodan, A., and Kenyon, C. (1997) *Science* **278,** 1319–1322
35. Ogg, S., Paradis, S., Gottlieb, S., Patterson, G. I., Lee, L., Tissenbaum, H. A., and Ruvkun, G. (1997) *Nature* **389,** 994–999
36. Giannakou, M. E., Goss, M., Junger, M. A., Hafen, E., Leevers, S. J., and Partridge, L. (2004) *Science* **305,** 361
37. Furuyama, T., Nakazawa, T., Nakano, I., and Mori, N. (2000) *Biochem. J.* **349,** 629–634
38. Ku, H. H., Brunk, U. T., and Sohal, R. S. (1993) *Free Radic. Biol. Med.* **15,** 621–627
39. Harman, D. (1956) *J. Gerontol.* **11,** 298–300
40. Beckman, K. B., and Ames, B. N. (1998) *Physiol. Rev.* **78,** 547–581
41. Bailey, C. J., and Ahmed-Sorour, H. (1980) *Diabetologia* **19,** 475–481
42. Tchernof, A., Calles-Escandon, J., Sites, C. K., and Poehlman, E. T. (1998) *Coron. Artery Dis.* **9,** 503–511
43. Heine, P. A., Taylor, J. A., Iwamoto, G. A., Lubahn, D. B., and Cooke, P. S. (2000) *Proc. Natl. Acad. Sci. U. S. A.* **97,** 12729–12734
44. Krege, J. H., Hodgin, J. B., Couse, J. F., Enmark, E., Warner, M., Mahler, J. F., Sar, M., Korach, K. S., Gustafsson, J. A., and Smithies, O. (1998) *Proc. Natl. Acad. Sci. U. S. A.* **95,** 15677–15682
45. Flurkey, K., Papaconstantinou, J., Miller, R. A., and Harrison, D. E. (2001) *Proc. Natl. Acad. Sci. U. S. A.* **98,** 6736–6741
46. Brown-Borg, H. M., Borg, K. E., Meliska, C. J., and Bartke, A. (1996) *Nature* **384,** 33
47. Bartke, A. (2000) *Results Probl. Cell Differ.* **29,** 181–202
48. Bartke, A., Wright, J. C., Mattison, J. A., Ingram, D. K., Miller, R. A., and Roth, G. S. (2001) *Nature* **414,** 412

ELSEVIER

Atherosclerosis 179 (2005) 345–351

ATHEROSCLEROSIS

www.elsevier.com/locate/atherosclerosis

Aortic pulse wave velocity and the degree of atherosclerosis in the elderly: a pathological study based on 304 autopsy cases

Motoji Sawabe[a,*], Ryutaro Takahashi[b,c], Satoru Matsushita[b], Toshio Ozawa[b], Tomio Arai[a], Akihiko Hamamatsu[a], Ken-ichi Nakahara[b], Kouji Chida[b], Hiroshi Yamanouchi[b], Shigeo Murayama[d], Noriko Tanaka[e]

[a] *Department of Pathology, Tokyo Metropolitan Geriatric Hospital, 35-2 Sakae-cho, Itabashi, Tokyo 173-0015, Japan*
[b] *Department of Internal Medicine, Tokyo Metropolitan Geriatric Hospital, Tokyo, Japan*
[c] *Human Care Research Group, Tokyo Metropolitan Institute of Gerontology, Tokyo, Japan*
[d] *Geriatric Neuroscience Research Group, Tokyo Metropolitan Institute of Gerontology, Tokyo, Japan*
[e] *Department of Biostatistics, Graduate School of Medicine, Tokyo University, Tokyo, Japan*

Received 19 December 2003; received in revised form 15 September 2004; accepted 30 September 2004
Available online 13 December 2004

Abstract

Introduction: Studies examining the correlation between aortic pulse wave velocity (PWV) and atherosclerosis have reported conflicting results. The present paper verifies this correlation by conducting autopsy examination of elderly subjects.
Methods: A total of 3456 PWV examinations had been performed on 1538 elderly people, as a part of routine physical check-up. During long-term follow-up, many of these subjects died, and autopsy study could be conducted on 304 of these subjects. The average age at death of the subjects was 83 years and the male: female ratio was 6:5. The pathological atherosclerotic index (PAI) was defined as the average pathological degree of atherosclerosis in eight large arteries, including aorta.
Results: Significant positive correlations were observed between the age and PWV ($\gamma = 0.273$, $P < 0.001$), and between the systolic blood pressure and PWV ($\gamma = 0.478$, $P < 0.001$). There was a significantly positive correlation between the aortic atherosclerotic degree and mean PWV ($\rho = 0.239$, $P < 0.005$), and between the PAI and mean PWV ($\gamma = 0.323$, $P < 0.001$). The partial regression coefficient between the PAI and mean PWV was 0.209, after adjusting for the mean systolic blood pressure and age at death.
Conclusion: The present study proved a weak correlation between the PWV and the pathologically verified degree of the aortic and systemic atherosclerosis.
© 2004 Elsevier Ireland Ltd. All rights reserved.

Keywords: Aging; Aorta; Atherosclerosis; Compliance; Elderly; Human; Pulse wave velocity

1. Introduction

The pulse wave velocity (PWV) is a marker of the elasticity of elastic or muscular arteries (aorta and its major branches), and reflects mainly the mechanical properties of the arterial wall. Diffuse sclerotic changes of the arterial wall observed in elderly or hypertensive cases increase the arterial stiffness. Meanwhile, the atherosclerosis is frequently associated with aging and hypertension. Although the atherosclerosis is initially localized to the intima, it finally affects the entire arterial lumen and results in medial destruction and fibrosis, and intimal calcification. Thus, the diffuse atherosclerosis likely causes the increase of arterial stiffness, especially in the advanced stage. Conflicting results have been reported on the correlation between the arterial stiffness and the severity of atherosclerosis. Avolio et al. reported that the PWV correlated well with the age in a northern Chinese community,

Abbreviations: BAI, brain atherosclerotic index; CSI, coronary stenotic index; PAI, pathological atherosclerotic index; PWV, pulse wave velocity

* Corresponding author. Tel.: +81 3 3964 1141; fax: +81 3 3964 1982.
E-mail address: sawabe@tmig.or.jp (M. Sawabe).

0021-9150/$ – see front matter © 2004 Elsevier Ireland Ltd. All rights reserved.
doi:10.1016/j.atherosclerosis.2004.09.023

known for its low serum cholesterol level and low prevalence of atherosclerosis in its population, and argued that atherosclerosis is therefore probably not the dominant factor responsible for the increase of PWV with aging [1,2]. Recent studies have reported that the PWV is high in cases with atherosclerotic complications, such as those with coronary heart disease and cerebrovascular disease, and that it is an important risk factor of cardiovascular mortality and primary coronary events, concluding that the PWV may indeed be a clinical marker of atherosclerosis [3–6]. Several trials of radiological evaluation of atherosclerosis by ultrasound, CT and MRI have been reported [7,8], and a significant correlation has been described between the PWV and surrogate radiological markers of atherosclerosis, such as the carotid artery intima-media thickness and plaques in the carotid arteries and aorta [9,10]. Since the degree of atherosclerosis differs from artery to artery, and even within the same artery, it is uncertain how reliably these radiological markers would reflect the degree of aortic or systemic atherosclerosis. Thus, the definitive and most direct assessment method of atherosclerosis still remains the pathological examination of resected arterial specimens or autopsy materials. However, no reports are available in the English medical literature that provides evidence of a positive correlation between PWV and the pathologically verified degree of atherosclerosis.

We performed PWV measurements as a part of routine physical check-up in a large number of elderly people and reported the results in a previous publication [11]. Many of these subjects died during long-term follow-up, and autopsy study could be conducted on some of them at our hospital. The present paper presents the results of a pathological study on the correlation between PWV and the severity of atherosclerosis, based on 304 elderly autopsy examinations.

2. Patients and methods

2.1. Patients

A total of 3456 PWV examinations were performed on 1538 unselected residents of Itabashi Home for the Aged, Tokyo, as a part of routine physical check-up between 1984 and 1996. During this period and subsequent long-term follow-up, some of these subjects died, and autopsy could be conducted in 304 cases among these residents at the Department of Pathology of Tokyo Metropolitan Geriatric Hospital, Tokyo, Japan. Both Itabashi Home for the Aged and Tokyo Metropolitan Geriatric Hospital are located in the same campus. The autopsy cases were composed of 165 males and 139 females. The age at death ranged from 67 to 103 years with an average age of 83 years. The most common cause of death was malignant neoplasms (29%), followed by infection (24%) and respiratory insufficiency excluding pneumonia (13%). Myocardial infarction and cerebrovascular disease were the main causes of death in 30 cases (10%) and 27 cases (9%), respectively. Aneurysmal rupture was found in seven

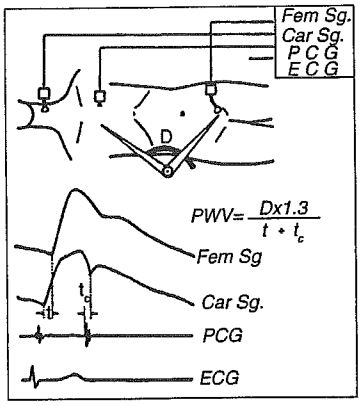

Fig. 1. Schematic diagram of the PWV measurement. Quoted from Figure 3 of the article no. [12] of the reference lists, by Yoshimura et al. by courtesy of the copyright holder. D, distance (in meters) from the second intercostal space at the right sternal edge to the point where the femoral pulse is palpated; 1.3 is a calculated constant of the ratio of the aortic length to D; t, the time interval (second) from the onset of the rapid ascending limb of the carotid pulse wave to that of the femoral pulse wave; t_c, central pulse wave transmission time (second), namely, the time interval from the beginning of the second heart sound to the notch of the carotid pulse wave.

cases (2%). Other diseases included gastrointestinal diseases (4%), renal failure (2%), hepatopancreatic diseases (1%), and miscellaneous conditions (6%). No cases of Takayasu's arteritis or Marfan's syndrome were included.

In the present study, the relationship between the results of PWV examination and the clinicopathological findings in these autopsy cases was analyzed.

2.2. Pulse wave velocity

The aortic, carotid-femoral PWV was measured by a tonometric method, using the Automatic Aortic Pulse Wave Velocity Meter (MCG400) manufactured by Fukuda Denshi Co. Ltd., Tokyo. According to Yoshimura's method [12], the PWV was calculated using the following equation: $\mathrm{PWV} = (D \times 1.3)/(t + t_c)$, and the schematic diagram of the PWV examination was shown in Fig. 1. The systolic and diastolic pressures were measured at these examinations. The reproducibility of the PWV measurement was checked by the review of 49 cases in which the PWV was measured twice at 4-month intervals. The correlation coefficient was high ($\gamma = 0.733$, $P < 0.0001$). The average values of the PWV and blood pressure were used for the statistical analyses, when the PWV examinations were repeated in any person.

2.3. Vascular pathology

After en-bloc extirpation of the cervical, mediastinal, retroperitoneal and pelvic organs at autopsy, the large arteries were cut open and fixed in 10% formalin solution. The severity of atherosclerosis was evaluated macroscopically by examination of their inner surfaces, except for the

case of the splenic and superior mesenteric arteries, which were evaluated on cut sections. According to modification of Gore–Tejada's atherosclerotic index [13], the atherosclerosis in the large arteries was semi-quantitatively scored on a scale of 0–8 according to the ratio of the atheroma-occupied area to the entire surface area: negligible (0 point, ratio = 0–1/20), minimal (2 points, 1/20–1/6), mild (4 points, 1/6–1/3), moderate (6 points, 1/3–2/3), and severe (8 points, 2/3–1). The large arteries examined included the common carotid artery, subclavian artery, aorta, splenic artery, superior mesenteric artery, common iliac artery, external iliac artery, and left femoral artery. In the case of bilateral arteries, the average score of the left and right sides was calculated. The term of "atheroma" was used in a broad sense, and it included fatty streaks, fibrous plaques, fibro-fatty plaques, and complicated lesions. It did not include mild diffuse intimal thickening, which is described as the aging phenomenon. Thus, the atherosclerotic changes could be differentiated from the aging changes of the arteries. The Pathological Atherosclerotic Index (PAI) was defined as the average value of the atherosclerotic scores in these eight large arteries. The PAI was calculated in 275 cases in which the atherosclerotic scores of all the eight arteries could be evaluated.

The Coronary Stenotic Index (CSI) was measured by one of the authors (K.C.), as previously reported [14,15]. Intracranial arteries were also semi-quantitatively examined by one of the authors (H.Y.), as previously reported [16]. The Brain Atherosclerotic Index (BAI) was defined as the average of the atherosclerotic scores of five intracranial arteries, including the anterior cerebral arteries, middle cerebral arteries, posterior cerebral arteries, basilar artery and vertebral arteries.

2.4. Statistical analysis

The atherosclerotic scores of individual arteries were compared by Friedman's test. The average values of the PWV and PAI were compared by Student's *t*-test or Welch's *t*-test. The atherosclerotic scores of the left- and right-sided arteries were compared by Wilcoxon's rank sum test. The correlations among the PWV, age at death, blood pressure, the atherosclerotic scores of individual arteries, and the PAI were studied by Spearman's rank correlation or Pearson's correlation. The correlation coefficients of Spearman's rank correlation and Pearson's correlation were designated as ρ and γ, respectively. Finally, a meta-regression method was applied to examine whether the changing rate of an individual's PWV was correlated with the PAI. The significance level was set at 0.05. The SAS system for Windows (Version 8.1) and StatView (Version 5.0) (SAS Institute Inc., NC) were used for the statistical analyses. The statistical analyses were performed by two of the authors (N.T. and M.S.).

2.5. Ethical considerations

Written informed consents were obtained from the bereaved family of the patients at the time of autopsy. The use of autopsy materials for medical education and research is generally permitted in accordance with the Act of Post-mortem Examinations of Japan.

3. Results

3.1. Pulse wave velocity

The histogram of the mean PWV showed normal distribution, with a mean (±S.D.) of 9.6 (±1.8) m/s. The mean PWV ranged from 5.1 to 14.3 m/s. About 61% of the cases showed abnormally high PWV values of more than 9 m/s. A total of 782 PWV examinations had been performed in the 304 autopsy cases. The average (±S.D.) and median numbers of PWV examinations per case were 2.6 (±1.9) and twice times, respectively. The largest number of examinations in one patient was 15 times. The intervals between the date of the last PWV examination and the date of death ranged from 10 days to 12.7 years. The average (±S.D.) and median intervals were 4.1 (±3.1) years and 3.5 years, respectively.

3.2. Clinical data and PWV

A positive correlation was observed between the age of the subjects at the time of the PWV examination and the PWV ($n = 3057$, $\gamma = 0.273$, $P < 0.001$). In the autopsy cases, a similar correlation between the age at death and the mean PWV was noted ($n = 304$, $\gamma = 0.250$, $P < 0.001$). When the last PWV data were applied in place of the mean PWV, weaker correlations were observed in the entire analysis. No significant sexual difference in the PWV was observed ($n = 304$, $P > 0.1$).

Histograms of the mean systolic and diastolic pressures and the mean pulse pressure showed normal distribution. The average pressures (±S.D.) were 146 (±20), 77 (±10), and 69 (±18) mmHg, respectively. A positive correlation was noted between the blood pressures and the PWV at all PWV examinations, as shown in Table 1. Similar correlations were observed between the mean blood pressure and the mean PWV in the autopsy cases.

Table 1
Correlations between blood pressure and the pulse wave velocity

	Correlation coefficients, (*r*)	*P*
All PWV examinations ($n = 3456$)		
Systolic pressure	0.478	<0.001
Diastolic pressure	0.294	<0.001
Pulse pressure	0.390	<0.001
Autopsy cases ($n = 304$)		
Mean systolic pressure	0.504	<0.001
Mean diastolic pressure	0.336	<0.001
Mean pulse pressure	0.370	<0.001

Values are Pearson's correlation coefficients between blood pressure and pulse wave velocity. PWV indicates pulse wave velocity.